Spring 2020

A Numerical Approach to Modeling Submoons and Investigating Stability Regions

Josephine Spiegelberg
jspiegelberg@rollins.edu

A Numerical Approach to Modeling Submoons and Investigating Stability Regions

A Senior Honors Project Submitted in Partial Fulfillment of
the Requirements of the Honors Degree Program

Josephine Spiegelberg

Faculty Sponsor: Dr. Christopher Fuse

Physics Department
Rollins College
Winter Park, Florida

April 17, 2020

I wish to express my gratitude for the encouragement, enthusiasm, guidance, and support of Dr. Christopher Fuse whose excitement for the subject was catching and without whom my time at Rollins would not have been the same. Thanks also to my committee Dr. Ashley Cannaday and Dr. Jay Yellen for your encouragement and helpful feedback.

I would also like to acknowledge the support of my friends and family, who shared the ups and downs of this process with me and without whom I would not be where I am today.

Contents

1 Introduction **1**

1.1 Impetus for Work 3

1.2 Moon Stability Studies 5

1.3 Submoon Stability Studies 17

2 Computational Methods for Studying Submoon Stability **25**

2.1 N-Body Legacy Code 25

2.2 Data Analysis Codes 29

2.3 Additions to the Code 30

3 Results **32**

3.1 Earth, Moon, Satellite System 32

3.2 Kepler 1625bi System 42

4 Discussion and Conclusion **53**

List of Figures

1 Moon Stability Regions as a Function of Planetary Mass, Stellar Mass, and Planetary Semi-major Axis 9

2 Stability Regions of Prograde Satellies as a Function of Satellite Semi-major Axis, Satellite Eccentricity, and Planet Eccentricity 13

3 Generalized Stability Regions of Pro- and Retro-grade Satellites as a Function of Satellite Semi-major Axis and Eccentricity 15

4 Lifetimes of Submoons as a Function of Submoon Semi-major Axis 19

5 Simplified Stability Regions of Submoons as a Function of Submoon Mass and Moon Semi-major Axis 20

6 Submoon Stability Regions Around Planets of the Solar System 24

7 Earth, Moon, Submoon in EMS System Motion in X-Y Relative to the Sun for 500 Year Timestep 33

8 Submoon in EMS System Motion in X-Y Relative to the Moon for 500 Year Timestep 34

9 Earth, Moon, Submoon in EMS System Motion in X-Y Relative to the Sun for 50 Year Timestep 35

10 Submoon in EMS System Motion in X-Y Relative to the Moon for 50 Year Timestep 36

11 Earth, Moon, Submoon in EMS System Motion in X-Y Relative to the Sun for 5 Year Timestep 37

12 Submoon in EMS System Motion in X-Y Relative to the Moon for 50 Year Timestep Over Time 38

13 Earth, Moon, Submoon in EMS System Motion in X-Y Relative to the Sun for 0.01 Year Timestep 39

14 Submoon in EMS System Motion in X-Y Relative to the Moon for 0.01 Year Timestep 40
15 Motion of Submoon in EMS System in X-Y-Z Relative to Sun for 0.01 Year Timestep 41
16 Motion of Submoon in EMS System in X-Y-Z Relative to Moon for 0.01 Year Timestep 42
17 Motion of Planet, Moon, and Submoon in Triton Configuration in X-Y Relative to the Star for 5 Year Timestep 44
18 Motion of Submoon in Triton Configuration in X-Y Relative to the Moon for 5 Year Timestep 45
19 Motion of Planet, Moon, and Submoon in Triton Configuration in X-Y Relative to the Star for 0.01 Year Timestep 46
20 Motion of Submoon in Triton Configuration in X-Y Relative to the Moon for 0.01 Year Timestep 47
21 Motion of Submoon in Triton Configuration in X-Y-Z Relative to the Star for 0.01 Year Timestep 48
22 Motion of Submoon in Triton Configuration in X-Y-Z Relative to the Moon for 0.01 Year Timestep 49
23 Motion of Planet, Moon, and Submoon in Ceres Configuration in X-Y Relative to the Star for 0.01 Year Timestep - Trial 1 51
24 Motion of Planet, Moon, and Submoon in Ceres Configuration in X-Y Relative to the Star for 0.01 Year Timestep - Trial 2 52

List of Tables

1 Possible Kepler-1625 b Configurations 4

2 Initial Orbital and Physical Parameters of Earth-Moon-Submoon Simulations 32
3 Initial Orbital and Physical Parameters of Kepler 1625-b System with Triton-like Submoon Simulations 43
4 Initial Orbital and Physical Parameters of Ceres-like Submoon 50

1 Introduction

In addition to the eight known planets in our Solar system, scientists have confirmed the existence of 4,172 exoplanets, or planets orbiting stars other than the Sun, and identified a further 2,522 exoplanet candidates [1]. The Solar system does not only contain planets, though, it is also home to approximately 214 moons [2] . These moons are believed to form either concurrently with the planet through accretion, or to be captured during the final stages of planet formation. The theories of planet formation are universally applied to all planets, as are those of moon formation. Thus, it is unlikely that the Solar system is special enough to be the only one with moons. Therefore, it is reasonable to hypothesize the existence of satellites orbiting exoplanets, also known as exomoons.

However, such satellites are small. Even within our own Solar system, the majority of the moons were identified long after the planets themselves [2]. The farther away from Earth we search, the more difficult it becomes to identify such bodies. In general, the search for exoplanets, and therefore exomoons, takes one of five forms: radial velocity, astrometry, direct imaging, gravitational microlensing, and transit. The term radial velocity refers to the radial velocity of a star caused by the gravitational force acting on it by an orbiting planet. This is seen from Earth via the Doppler shift that this velocity causes in the light emitted by the star. The change in velocity of the star due to an exoplanet may also be observed based on the miniscule motions of the star relative to other stars in the vicinity in a process known as astrometry, though this requires particularly precise optics. The next method of exoplanet identification is direct imaging, which images exoplanets by reducing the signal from the star in order to see the weaker signal from the planet itself. Gravitational microlensing works by taking advantage of the distortion of light due to the gravity of a massive object. As with a lens, when the gravity of one body focuses the light emitted by another, the farther body's signal on Earth is increased. Planets orbiting this heavy body

also lens the light, causing a spike in the light signal from the star. Finally, an exoplanet may be identified when it passes directly between its host star and the observer on Earth. When this occurs, the light signal from the star is reduced by a measurable amount. This method was used, for example, by NASA on their Kepler mission which ran from 2009 to 2013 and found thousands of exoplanet candidates [3].

In October of 2018, Alex Teachey and David Kipping published evidence for the discovery of the first-ever exomoon candidate. The finding was based on transit data from the Kepler mission supplemented by images gathered by the Hubble Space Telescope [4]. The exomoon candidate is believed be orbiting the gas giant planet, Kepler-1625b. Data suggests that Kepler-1625b is several times the mass of Jupiter, while the exomoon likely has a Neptunian mass and radius. These results follow from fitting of the light curve and modeling of the theorized light curve for various potential bodies orbiting Kepler-1625b [4].

The potential exomoon is particularly large, especially when compared to the moons in the Solar system. Of these, the majority orbit the planets of the outer Solar system, Jupiter, Saturn, Neptune, and Uranus, which also host the largest moons. Among the largest are Ganymede, which orbits Jupiter and is 2.4 times smaller than Earth [5], Titan, which orbits Saturn and is 2.5 times smaller than Earth [6], and Callisto, which orbits Jupiter and is 2.6 times smaller than Earth [7]. Thus, the largest moons in the Solar system do not approach the size of this proposed Neptunian satellite, which is approximately 3.9 times larger than the Earth [8]. The large size of this potential exomoon raises the possibility of further satellites orbiting it. After all, if the planet Neptune hosts 14 regular moons [2], a Neptune-sized moon might host its own moons as well. If such submoons exist, what are the conditions under which they would be stable?

The purpose of this work is to review existing literature on theoretical satellite-orbiting bodies, or submoons, and to model these bodies in order to constrain stability conditions.

In order to achieve this goal, the stability conditions and formation conditions for moons

will first be investigated. This process will identify stability factors that may be applied to the study of submoons. In addition, the characteristics of the exomoon candidate, Kepler 1625-bi, will be reviewed in order to provide further context for a potential submoon in this system.

Finally, the impact of stability criteria for submoons will be tested by simulating a submoon system. These simulations will be achieved using an N-Body Fortran code, which calculates the positions and gravitational interactions between initialized bodies.

1.1 Impetus for Work

Because submoons have not been observed in our Solar system, there has been little impetus to study them in the past. However, a relatively recent exoplanet survey has revealed a potential exomoon candidate orbiting the planet Kepler 1625-b. This planet was identified in 2018 based on data collected by the Kepler space telescope, wherein the light signal emitted from the star Kepler 1625 was analyzed for periodic light occultations due to a passing planet [9]. This signal revealed telltale signs of a transiting planet, with an additional abnormality in the light curve. This abnormality led to the targeted observation of three further transits by Teachey et al. [4] which revealed the potential presence of an exomoon. The potential orbital parameters of the exomoon were very loosely constrained by the data, as many different configurations of the planet and exomoon system were theoretically possible. The initial lightcurves could fit many configurations ranging from a Saturn-mass planet with an Earth-mass moon to a very low-mass star with a Neptune-mass planet and no moon at all, which are summarized in Table 1 (Table 1 of Heller 2018). However, Heller (2018) identified the configuration, dubbed TKS, to be the most likely constellation of planet and moon masses [9]. This configuration consisted of a G-type star, with a surface temperature of between 5,000 and 6,000 Kelvin, a planet with a radius similar to that of Jupiter, and a moon with Neptune-like dimensions [4].

Scenario	$R_\star$ [$R_\odot$]	R_p [R_{Jup}]	R_s [R_{Jup}]	M_p [M_{Jup}]	M_s [$M_\oplus$]	M_s/M_p
(1aa) Saturn-mass gas planet, Earth-mass gas moon	1.305[a]	0.86[b]	0.26[b]	0.4[3]	1[1]	7.9×10^{-3}
(1ab) Saturn-mass gas planet, Neptune-mass water–rock moon					17[2]	1.3×10^{-1}
(1ba) brown dwarf, Earth-mass gas moon				75[3]	1[1]	4.2×10^{-5}
(1bb) brown dwarf, Neptune-mass water–rock moon					17[2]	7.1×10^{-4}
(2aa) very-low-mass star, mini-Neptune planet	1.793[a]	1.18[b]	0.35[b]	91[3]	10[4]	3.5×10^{-4}
(2ab) very-low-mass star, super-Earth water–rock planet					70[2]	2.4×10^{-3}
(3aa) very-low-mass star, Neptune-like planet	2.056[a]	1.36[b]	0.40[b]	112[4]	20[4]	5.6×10^{-4}
(3ab) very-low-mass star, super-Saturn water–rock planet					180[2]	5.1×10^{-3}
(TKS) super-Jovian planet, Neptune-like moon	–	1[5]	0.35[5]	10[5]	17[5]	5.4×10^{-3}

Notes. [(a)] The stellar radius estimates are based on Mathur et al. (2017). [(b)] The radii of the transiting primary and proposed secondary were estimated from the lightcurves of Teachey et al. (2018). The corresponding masses of the objects were estimated using structure models and evolution tracks from the following references.

References. (1) Masuda (2014); (2) Fortney et al. (2007); (3) Baraffe et al. (2003); (4) Baraffe et al. (2008); (5) Teachey et al. (2018).

Table 1: This table, from Table 1 of Heller (2018), lists the possible configurations for Kepler-1625 b and its proposed moon based on fitting of the observed lightcurve. The scenarios are classified by the necessary radii of the star, planet, and satellite. The TKS solution based on the work of Teachey et al. (2018) [4] is presented in the last row, and was determined to be the most likely constellation of planet and moon masses and radii [9].

Based on these data, Teachey et al. (2018) proposed additional observations of the Kepler 1625 system using the Hubble Space Telescope (HST). The HST data provided strong statistical evidence in favor of the existence of an exomoon, though not definitive proof due to the unknown systematic errors in the data [10]. The Teachey et al. (2018) fit to the new transit data predicted a planet with a largely circular orbit about one astronomical unit (AU) from the star, placing it a semi-major axis comparable to that of the Earth. This planet was found to be approximately 103 Earth masses, or several Jupiter masses, and to have a gravitational sphere of influence reaching out to 200 $\pm$ 50 planetary radii. Additionally, it predicted an moon orbiting this planet on a very wide orbit of about 40 planetary radii. This moon was also modeled to have a radius about four times the Earth's radius. However, the constraints on the moon were relatively weak, as there was a prograde and retrograde orbital degeneracy and a possibility that the moon was moving on a 45° orbit rather than a coplanar with the planet [11].

Despite the lack of orbital constraints, the large size and wide orbit of the proposed

exomoon is highly unique. In fact, a Neptune-sized moon with a large semi-major axis could even be able to host its own moon, or submoon. The proposal of this new exomoon has thus led to a new wave of interest in potential submoons, which had thus far not been studied much as they have not been observed in our own Solar system.

Interestingly, a subsequent study of the Kepler and HST data collected by Teachey et al. (2018) resulted in a very different conclusion. Kreidberg et al. (2019) reanalyzed light curve data and found that their model indicated a better fit with a planet-only solution. They postulated that Teachey et al.'s exomoon candidate was purely a product of data reduction rather than a physical phenomenon [12]. Teachey et al. addressed these concerns and found that the new reduction by Kreidberg et al. was a less accurate fit, as it had higher intraorbit and post-fit residual scatter for example. They argued that these problems can be explained by systemic problems in Kreidberg's reductions and that their own initial fit with the planet-moon system was more accurate [13]. Overall, more analysis from other research groups will help to either prove or disprove the existence of this large exomoon.

Regardless of the existence of the exomoon Kepler 1625-b i, it's mere theorization has sparked interesting research into the nature of submoons, where there is much to be explored.

1.2 Moon Stability Studies

As many of the factors affecting the stability of moons may be paralleled in the search for the stability criteria of submoons, it is useful to summarize past research into moon stability. Findings on moon stability can be used to inform the direction of submoon research as more parallels are drawn between the two.

In its most basic form, the calculation of moon stability is based on the restricted three-body problem, wherein the gravitational interactions of three bodies, each orbiting another, are calculated. This problem is highly complex and cannot be directly solved. Rather, it is modeled through computational simulations. However, when the mass of the second body,

in this case the planet, is assumed to be very small compared to the mass of the first body, the star here, the problem can be simplified to a two-body problem. When even further simplified so that the moon is much smaller than the planet, the motion of the smaller mass around the larger mass can be described in cartesian coordinates by the equations

$$\ddot{x} - 2\dot{y} = \left(3 - \frac{\mu_3}{\Delta^3}\right) x, \tag{1}$$

and

$$\ddot{y} - 2\dot{x} = \left(-\frac{\mu_3}{\Delta^3}\right) y, \tag{2}$$

where μ_3 is the mass of the smaller body times the gravitational constant G and $\Delta^2 = x^2 + y^2$ [14].

Solving these differential equations yields a zero-velocity surface around the larger object, upon which the smaller body's velocity is zero. This surface bounds the sphere of gravitational influence around the larger body, commonly referred to as the Hill sphere. The radius of this sphere can be approximated as,

$$\Delta H \approx a(1-e)\frac{\mu_3}{3}^{\frac{1}{3}}, \tag{3}$$

where ΔH is the Hill radius, a is the semi-major axis of the larger body, e is the eccentricity of the larger body's orbit, and μ_2 is the mass of the larger body [14]. Thus, the sphere of gravitational influence of a planet, for example, grows as the planet's orbital radius increases, as the planet's orbit becomes more circular, and as the planet's mass increases. Of course, though this analysis provides a useful starting point for understanding some of the factors of moon stability, it is highly simplified. Both more complex theoretical calculations and simulations provide more insight into how different processes and bodies can affect moon stability.

Such research has shown that the stability of moons is strongly dependent on the characteristics of the parent star, the physical and orbital parameters of the planet, and the migration and scattering history of the planet. Of course, characteristics of the moons themselves, such as their size, location, inclination, and the orbital motion relative to planetary rotation, are incredibly important factors in moon stability. Understanding these factors in moon stability will provide valuable insight into the factors impacting submoons along with providing guidance for future submoon stability research.

Overall, planets with low eccentricities, large masses, wide orbits, and no history of migration or scattering are most likely to host stable moons. Furthermore, close-in moons with low inclination and low eccentricity orbits are more likely to be stable, and moons on retrograde orbits are more stable on very wide orbits than prograde moons. Planets orbiting close to heavy stars are also more likely to host stable moons. The influence of moon mass is unclear, as some research shows low mass moons to be more stable while other work finds larger moons more stable.

The nature of the parent star around which satellites orbit can greatly affect their stability. For example, stars can drive photoevaporation that causes planetary mass loss. This mass loss can cause moons to become unstable as the Hill sphere of the planet shrinks and moon orbits expand and become more eccentric. The photoevaporation process is closely tied to the star itself, as X-ray luminous stars more easily drive photoevaporation than others. Thus, it can be expected that moons around such stars are less likely to exist on long-term stable orbits [15].

In addition to photoevaporation, the star around which a moon orbits causes stellar tides on the planet. These tides can slow a planet's rotation and lead to the removal of satellites through tidal migration [16]. Simulations have demonstrated that the absence of satellites around Mercury and Venus can be accounted for by tidal interactions with the Sun [17, 18]. Barnes & O'Brien (2002) found that for a large stellar mass, more than 1.5 times our

Sun's mass, Jovian planets can retain stable Earth-mass moons for approximately 5Gy [16]. However, by combining these stellar tides with lunar tides from orbiting satellites, Sasaki et al. showed that that lighter parent stars host more stable moons. Thus, they conclude that moons are generally more stable around lower mass M-type stars than G-type [19].

Thus, the luminosity and mass of a star can affect the stability of satellites through the influence of photoevaporation and stellar tides.

While the nature of the host star is certainly an important factor in moon stability, the size, location, and eccentricity of the parent planet must also be considered. Just as photoevaporation and the resulting loss of planetary mass is affected by the nature of the star, it is also affected by the location of the planet itself relative to the star. Kohler (2017) found that the destabilization of moons through photoevaporation is more exaggerated for planets located less than 1 AU from the host star [15]. In addition, when considering tidal forces, Sasaki et al. (2012) found moons to be more stable when orbiting more massive planets further from the star [19]. Thus, satellite stability is increased around planets with larger semimajor axes when a variety of influences are considered.

In 2002, Barnes & O'Brien considered specifically the stability of satellites around close-in planets with a semi-major axis of less than 0.6 AU. In the resulting model, the stable region around a planet was directly related to its mass and semi-major axis as shown in Figure 1, below (Fig. 3 of Barnes & O'Brien 2002). The three lines in Figure 1 show the minimum planetary masses that can host moons with masses comparable to the Moon, Mars, and Earth with a duration of 5 Gyr as a function of planetary semi-major axis and stellar mass. In the Barnes & O'Brien model, as the stellar mass increases, moons are more stable, as discussed above. In addition, as the planet mass increases, the stability region for each moon mass increases as well. Finally, as the planet's semi-major axis increases, the stability regions also increase [16]. These findings are in agreement with the Hill radius given by Equation 3: bodies with larger masses have larger Hill spheres, as do bodies with larger semimajor axes.

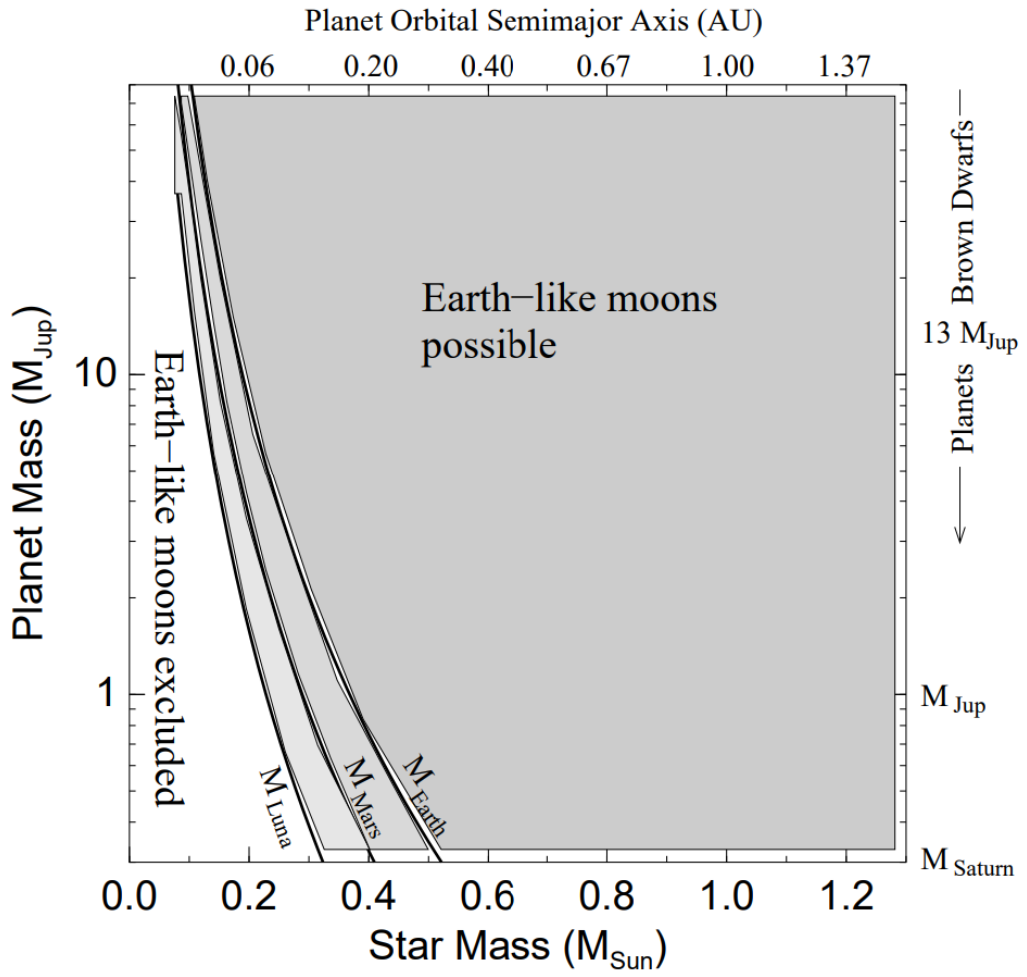

Figure 1: This figure from Figure 3 of Barnes & O'Brien (2002) shows the stability region of Earth-like moons as a function of planet mass, star mass, and planet semi-major axis. The three lines indicate the minimum planetary masses necessary to host moons with masses comparable to the Moon, Mars, and Earth for 5Gyr [16].

In addition to the location of the planet relative to the star, the location of the planet relative to other planets can also be critical for moon stability. In their analysis of the stability regions around giant planets in our Solar system, Shen & Tremaine (2008) found that gravitational perturbations from other planets greatly affect stable zones beyond the Hill sphere [20]. Furthermore, Domingos et al. (2006) described stability as a function of

planetary eccentricity, as shown in Figure 2 (Figure 2 of Domingos et al (2006)) [21]. Shen & Tremaine found that as the eccentricity of the planetary orbit increases, the stability region and critical semi-major axis for both pro- and retrograde satellites decreases [20]. This result makes sense, as a planet with an increased eccentricity undergoes large variations in gravitational forces over the course of a single orbit.

Thus, more massive planets at larger semi-major axes with lower eccentricities have been found to host more stable satellites. The location of the planet relative to other planets in the system can also cause gravitational perturbations that shape stability regions beyond the Hill sphere.

In addition to its inherent characteristics, the host planet's past also plays an important role in the presence of stable moons in orbit around it. This is an important consideration for moon stability, as planetary migration is believed to be a very common occurrence. In fact, the majority of the planets in the Solar system are theorized to have undergone significant orbital migration during their formation [22].

One method of forming close-in giant planets, like those investigated by Barnes & O'Brien (2002) or Kepler 1625-b, is through inward, or Type I, migration during the last stages of planet formation. These planets are believed to form outside of the ice line and then migrate inwards. As the planets experience a decreasing semi-major axis, their Hill sphere shrinks and it becomes harder to gravitationally preserve their satellites. Interestingly, because the planetary migration timescale is so much larger than the moon's orbital period, 106 years compared to about 102 days, the moon's orbit is not directly affected by the migration and the instability is mainly a result of the evolution of the Hill sphere [23]. Of course, there are other processes affecting moons during migration. Notably, as a planet migrates, moons orbiting within approximately 10 planetary radii may be caught in an evection resonance, whereby their orbital eccentricities grow dramatically, resulting in a collision with the planet. The exact boundary for moons caught in this resonance depends on the mass, oblateness, and

size of the migrating planet. Some moons are able to survive an evection resonance depending on the timing of the migration and inter-lunar perturbations [24]. Thus, planetary migration can have enormous effects on satellites and the presence of satellites around newly discovered planets can provide insight into their formation process.

Within the population of observed giant exoplanets, there is a broad eccentricity distribution. One possible explanation for this distribution is planet-planet scattering. This process has a largely detrimental effect on existing satellites. Through N-Body simulations, Hong et al. (2018) found that approximately 80 to 90% of moons were destabilized in planet-planet scattering simulations. While the survival of moons did have a strong radial dependence, even close-in moons only had a 20-40% survival rate. The survival rate also increased with host planet mass, which makes sense considering Equation X for the Hill sphere [25]. Because of the low survival rate of moons during scattering, observations of exomoons, or a continued lack thereof, will provide more insight into the role of scattering in exoplanet formation.

Though the results of Hong et al. (2018) virtually precludes scattered planets from retaining moons, Barr et al. (2017) have proposed a solution through which scattered planets may still host moons. They show that when two rocky planets with masses between 0.25 and 10 Earth masses collide, a debris disk may be created from which new satellite systems could accrete. Disk formation requires collisions at oblique angles and velocities near the escape speed, and the mass of the disk is directly related to the impact velocity and angle, increasing for high velocities and glancing impacts. The mass of the colliding planets also affects the disk mass, as interactions between planets of equal masses create larger debris disks. A more massive disk allows for more massive moons to form [26]. Thus, though existing moons may not be retained through planet-planet scattering, these collisions could result in new moon formation through the creation of a debris disk.

Perhaps the most important factor in moon stability, however, is the nature of the moon itself. A close-in moon on a low-inclination, circular orbit, is generally found to be stable

under a variety of conditions. In addition, the study of pro- and retrograde moons has revealed that retrograde satellites generally have larger stability regions than prograde satellites (Domingos et al. 2006). The impact of moon mass is dependent on the situation being studied, when photoevaporation is taken into account, smaller moons are found to have a higher survival rate [27], while tidal studies find that heavier moons are more stable if the moon and planet are tidally locked but less stable if this does not occur [16]. Thus, more research into the impact of satellite mass on stability when many factors are accounted for is needed.

Through numerical simulations of the restricted elliptic three-body problem, Domingos et al. (2006) calculated the borders of the stable regions of prograde satellites around planets of various eccentricities as shown in Figure 2. In these simulations, the satellite was modeled as a low mass test body on a fixed orbit. Domingos et al. (2006) found that in the large majority of cases, a stable region exists for orbits close to the planet, and as the stable region shrinks with increasing satellite and planet eccentricities, the allowed satellite semi-major axis is reduced [21].

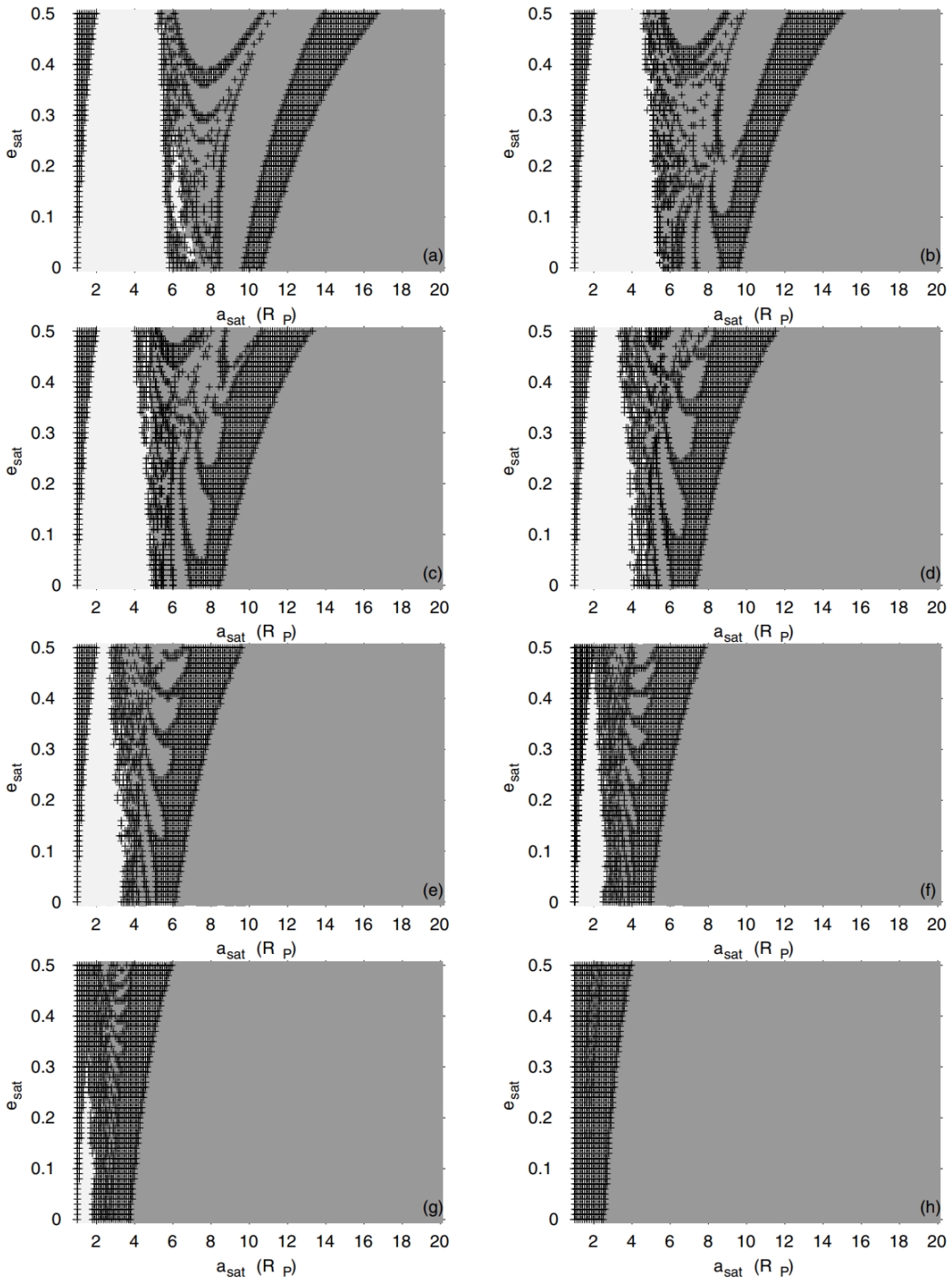

Figure 2: This figure from Figure 2 of Domingos et al. (2006) shows the stability regions of a prograde satellite as a function of satellite semi-major axis, satellite eccentricity, and planetary eccentricity. The + symbol indicates collisions of the satellite and the dark areas correspond to unstable regions, while the white areas correspond to stable regions [21].

Furthermore, Domingos et al. (2006) found that as satellite eccentricity increases, the stable region tends to shrink as well. Interestingly, in comparing prograde satellites, which orbit in the same direction as the planet's rotation, with retrograde satellites moving in the opposite direction, it was found that retrograde satellites tend to have a larger stability region. In fact, the stability region for a retrograde satellite with a low planetary eccentricity was found to extend past the Hill sphere of the planet, as shown in the right image of Figure 3. These additional stable regions correspond to the F family of periodic orbits [21]. The final expressions for the outer bounds of the stability regions for prograde and retrograde satellites are given in terms of the Hill radius of the planet (Eq. 3) by

$$a_{EPro} \approx 0.4895\,(1.0000 - 1.0305 e_P - 0.2738 e_{Sat})\,, \tag{4}$$

and

$$a_{ERet} \approx 0.9309\,(1.0000 - 1.0764 e_P - 0.9812 e_{Sat})\,, \tag{5}$$

where e_P is the planetary eccentricity and e_{Sat} is the satellite's eccentricity [21]. The inner boundary of the stability region was determined by

$$R_p = a\,(1 - e_{Sat})\,, \tag{6}$$

for both cases [21]. This study provides useful guidelines for moon stability in the most general situation.

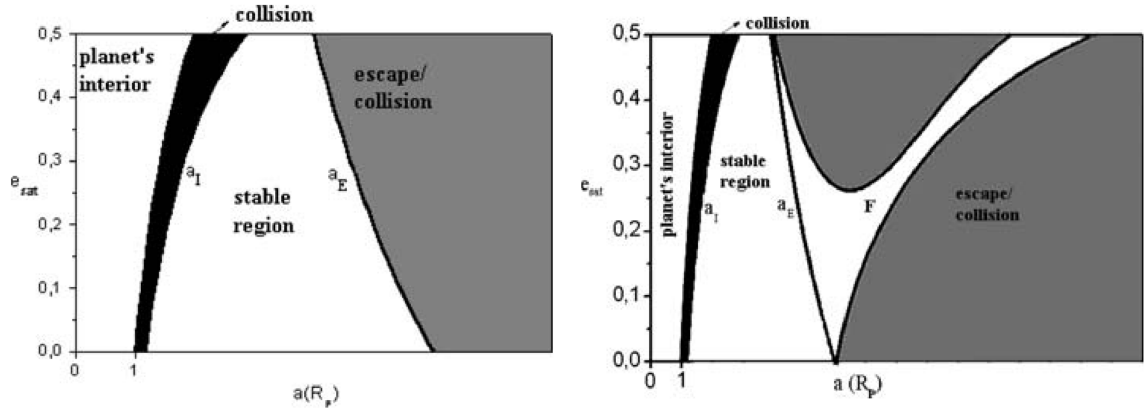

Figure 3: These figures from Figures 4 and 5 of Domingos et al. (2006) show the generalized stability regions of prograde (left) and retrograde (right) satellites as a function of satellite semi-major axis and eccentricity. The white stable regions are bounded on the left by Equation 6 and on the left by Equations 4 and 5 respectively. The addition stability region in the prograde case is denoted by the letter 'F', as it is associated with the F family of periodic orbits [21].

Studies considering further influences on moon stability, such as photoevaporation or tidal forces, generally agree with the results of Domingos et al. (2006), but they are able to expand more on the impact of inclination, tidal forces, and other gravitational interactions between planets. For example, in a 2008 study on distant gas giants in our Solar system, Shen & Tremaine found that within the planets' Hill spheres, no stable orbits existed for moons with high inclinations relative to the planet's orbital plane [20]. The destruction of moons on high inclination orbits is likely due to so-called Kozai oscillations, which result in moons on orbits in close proximity to the planets. When they are this close to the planet, the moons are strongly affected by tidal evolution and disruption, causing direct collisions between the satellite and the planet [28]. Thus, the impact of satellite inclination on stability is an important factor when searching for stable regions.

In addition to investigating the impact of inclination, the Shen & Tremaine (2008) study took into account the effects of gravitational interactions on satellites of the giant plants in our Solar system. They found that prograde satellites were stable up to smaller semi-major

axes than retrograde satellites, with values similar to those found by Domingos et al. (2008). Specifically, they determined that many prograde satellites can survive out to about half the Hill radius, while retrograde satellites can survive to circa 0.7 to 1 times to Hill radius [20]. In addition, Domingos et al. found that some coplanar satellites had stable orbits at semi-major axes greater than twice the Hill radius for Jupiter, Uranus, and Neptune. Surprisingly, Uranus and Neptune actually had some stable orbits with radii up to 10 times the Hill radius. Domingos et al. determined that differences in stable orbits outside the Hill sphere between the planets could be attributed to gravitational perturbations between planets and differences in the planet-to-Sun mass ratios [21]. Thus, gravitational interactions between planets must be considered when studying the stability of retrograde satellites outside the Hill sphere.

In constructing their stability regions, both Domingos et al. (2006) and Shen & Tremaine (2008) did not account for variations in satellite mass, instead treating the satellite as a test particle with negligible mass [21, 20]. These, however, become important when considering the influence of photoevaporation, tides on the moons, or systems with multiple moons of varying masses. When photoevaporation occurs, as discussed earlier, most satellites are destroyed, but in about 25% of cases, small close-in satellites survive. Therefore, when photoevaporation is a dominant process, it greatly shrinks the range of possible semi-major axes and satellite masses. Similarly, when tidal processes are accounted for, the mass of the satellites has an impact on its stability. Barnes & O'Brien (2002) find that more massive satellites are removed more quickly by stellar tides and migration effects than less massive moons around close-in planets [16]. In 2012, Sasaki et al. expanded on this work, finding that the stability of moons is linked to tidal locking. They identified three main tidal locking patterns: the planet locks with the star and then the moon, the planet locks only with the moon, or the planet and moon are never tidally locked. Sasaki et al. (2012) found that massive moons are more stable and have a longer lifetime for the first two cases, while they have a shorter lifetime in the last case, where they are never tidally locked with the planet

[19]. Thus, different tidal interactions can have varying effects on the stability of massive moons as opposed to smaller satellites. Overall, introducing other influences on satellites can provide insight into the importance of mass for moon stability.

The regions where moons can survive are impacted by a large variety of factors based on the characteristics of the star, planet, and moon itself. Specifically, moons are found to be more stable around distant planets with low eccentricities, large masses, and no history of migration of scattering. In addition, they are generally more stable on close-in or retrograde orbits with a low inclination and a low eccentricity. The impact of the mass of the star and the moon itself depend heavily on the dominant conditions affecting the moon. These factors for moon stability can be adapted to understand submoon stability by simply replacing the star with a planet, the planet with a moon, and the moon with a submoon.

1.3 Submoon Stability Studies

In the past, some research has been done to narrow down stability conditions for submoons and how they relate to the stability of moons. This research is, however, rather limited as there was not much impetus to study submoons before the discovery of exomoon candidate Kepler 1625-b i. Interestingly, some work was done on this topic in the 1970s and 1980s, when it was theorized that the moon's craters could be the result of submoons colliding with the lunar surface [29, 30].

Submoon research has drawn many parallels to moon stability. The most recent work suggests studying the stability of satellites around close-in planets with short periods is especially useful, as the stability regions for moons orbiting planets have much smaller radii than those of planets orbiting stars [31]. In general, the factors found to impact the stability of submoons have mirrored those affecting the stability of moons, with some exceptions. Through limited studies, it has been found that submoons can be stable on low eccentricity, low inclination, wide radius orbits around moons also on a wide orbit. In addition, a low

mass ratio between the submoon and its parent moon has been shown to lead to more long-term stability. However, the study of submoons has thus far been incredibly limited and there are many mechanisms and factors that have yet to be considered.

Though the majority of submoon research is well-correlated to moon research, one of the main exceptions is the impact of the submoon semi-major axis. When a multitude of factors, such as photoevaporation, migration, and tidal influences, are considered, moons on close-in orbits have been found to be generally more stable. However, submoon research thus far has shown that a large submoon semi-major axis corresponds to a longer lifetime [29, 30]. This finding can be seen in Figure 4 (Fig. 3 of Reid 1973), where the lifetimes of theoretical objects orbiting our Moon are plotted with respect to their initial semi-major axis for various submoon-moon mass ratios [29]. For each plotted mass ratio, the lifetime of the submoon increases as the submoon semi-major axis increases. Thus, submoons on wider orbits are stable for longer timescales than those on close-in orbits. These findings are also reproduced in a more recent study, where Kollmeier & Raymond (2019) showed that 10-km submoons could be stable around large moons only on wide-separation orbits [31]. Of course, there are limitations to these studies: both Reid and Conway's research was conducted without many modern computational advancements which heavily limited the scope of their work, and Kollmeier & Raymond's work is meant only as a broad early investigation into submoon stability. These limitations may also explain why these submoon findings do not align with the corresponding findings for moons. Thus, though these works provide useful first steps, future work is required to fully understand the impact of a submoon's semimajor axis on its stability.

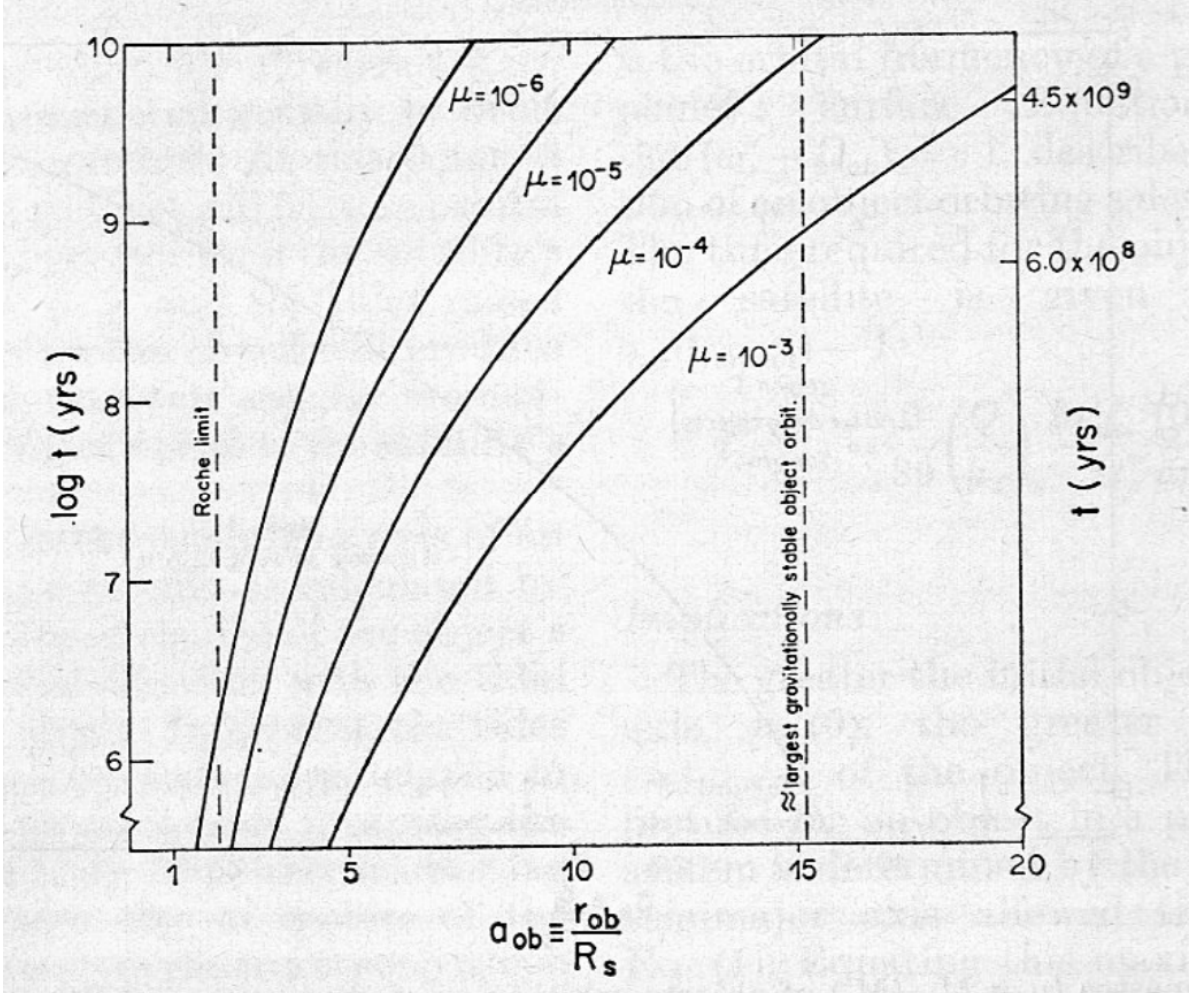

Figure 4: This figure from Figure 3 of Reid (1973) shows the lifetimes of bodies with various masses orbiting the moon as a function of their initial scaled semimajor axis, a_{ob}. Each line on the plot corresponds to a different mass, where $\mu = M_{object}/M_{moon}$ [29].

When considering moon stability, one of the most important factors is the planet's orbit, including its eccentricity, inclination, and semi-major axis. The planet's orbital radius is analogous to the moon's semi-major axis when studying submoons. A planet on a wider orbit is able to host moons in a larger region, as it has a larger Hill sphere given by Equation 3. This behavior has thus far been mirrored in submoon studies. In 1973, Reid found that the number of stable mass ratios increases as the moon semi-major axis increases, and that there is a critical moon semi-major axis below which no submoons can be stable, as shown

in Figure 5 (Fig. 2 of Reid 1973) [29]. In addition, Kollmeier & Raymond showed recently that moons on wide orbits are most likely to host a stable submoon [31]. Thus, preliminary research indicates that moons with large orbital radii are best suited to hosting submoons.

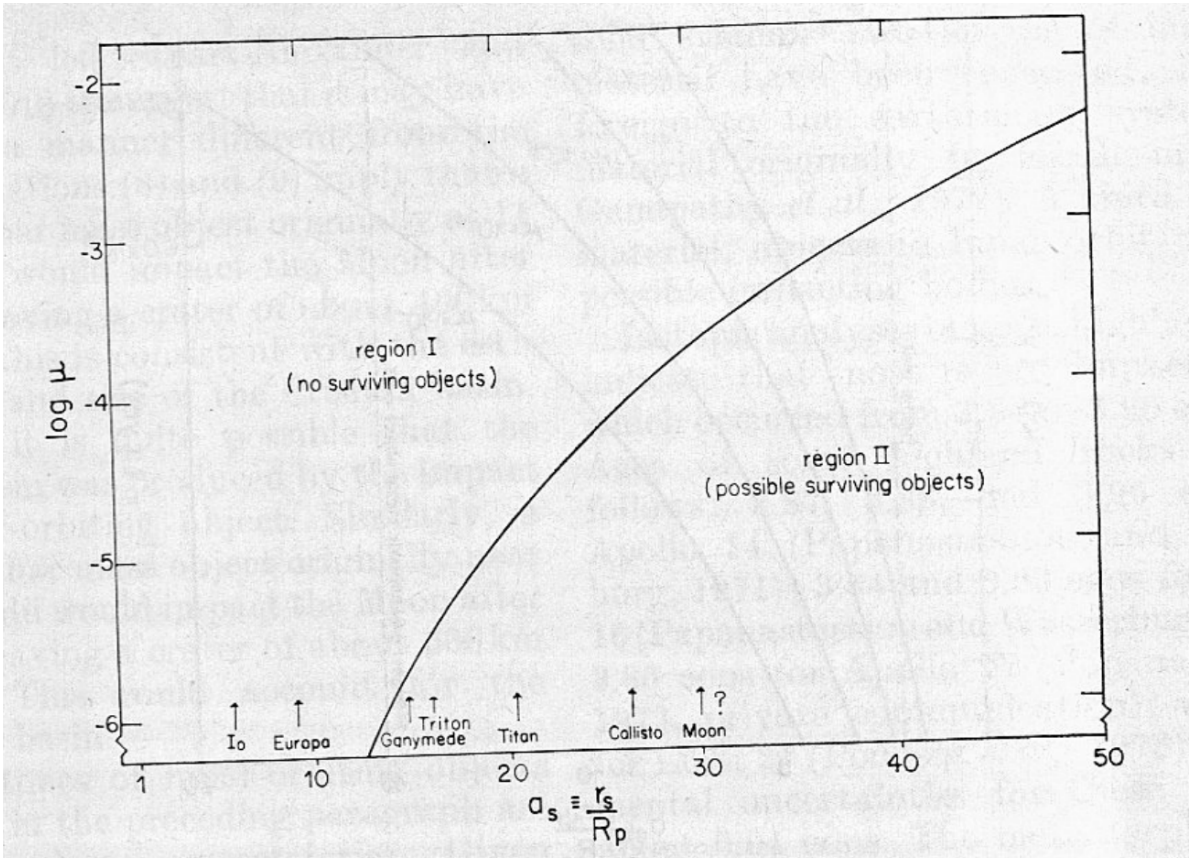

Figure 5: This figure, from Figure 2 of Reid (1973) shows the theoretical stability regions of submoons as a function of the relative submoon mass ($\mu = M_{submoon}/M_{moon}$) and the scaled moon semi-major axis ($a_s = \frac{r_s}{R_p}$). Region I describes the area where there are no stable submoons, while Region II describes the area where submoons could survive. Some moons of the Solar system are shown for comparison [29].

Another main focus of both moon and submoon research is the mass of the bodies involved (i.e. planet and moon and submoon). Of course, when investigating submoons, there are three bodies to consider, instead of the two bodies interacting in the planet-moon system. The addition of this third body, greatly complicates the system. After all, the so-called "three-body problem" in classical mechanics has no general closed-form solution, and for the

majority of initial conditions the resulting system is chaotic and requires numerical methods to be solved [32]. In the past, submoon research has circumnavigated this problem either by assuming that each mass is much larger than the next, or by treating the masses as point sources [29, 30, 31].

Thus far, submoon research has focused heavily on the mass ratio between the moon and submoon, rather than their individual masses. Recent results show that small submoons, as compared to their host moon, are stable over a wider range of moon semi-major axes and for a longer lifetime [29, 30]. As seen in Figures 4 and 5, a study of a small number of ratios shows that higher mass ratios result in decreased submoon lifetimes and smaller stability regions. In Figure 4, the curves indicate different submoon-moon mass ratios. Larger mass ratios correspond to larger submoons in relation to the moon. Here, it can be seen, that as the mass ratio increases, the curve becomes flatter, indicating that submoons survive for a shorter period of time at large orbital radii. Similarly, in Figure 5, the mass ratio between the submoon and the moon is plotted on the y-axis while the moon's semi-major axis is plotted on the x-axis. For large mass ratios, the region of possible surviving objects shrinks. In fact, as the mass ratio increases, the necessary moon semi-major axis for a stable submoon also increases [29]. In contrast to historical studies, Kollmeier & Raymond (2019) were able to study the individual masses of the moon and submoon. They found that smaller submoons are stable over a broader range of moon radii and semi-major axes, while larger moons are also more likely to host stable submoons [31]. Thus, both historical and more recent submoon studies show the increased stability of small submoons orbiting relatively massive moons.

Counterintuitively, Conway (1985) also identified a critical submoon mass below which submoons are not stable at a given eccentricity and semi-major axis. This critical submoon mass results from the study of 'Hill Type' stability, which does not account for orbital evolution over time, tidal forces, or interactions from other bodies [30]. Thus, though Conway

does identify a minimum submoon mass, this mass is based on highly simplified calculations and should be further studied through simulations that take many more factors into account.

In addition to the intrinsic properties of the bodies such as the planet, moon, or submoon, there are processes that may affect the stability of moons, and therefore probably submoons as well. Though many of these processes have yet to be investigated in the context of submoons, the impact of tidal forces on submoons has been studied to an extent. Just as tides on a moon from its host planet cause it to undergo tidal migration, thereby removing its moons [16], tides on submoons from host-moons also cause orbital decay [29]. Reid found that when the moon's spin frequency is below the submoon's orbital frequency, tides from the moon, 'drain' the orbital angular momentum of the submoon and cause tidal decay. This may lead to destabilization of submoons and eventual collisions with the moon itself. In contrast, Conway (1985) found that tides actually circularize the submoon's orbit and have a stabilizing effect [30]. These opposing findings are the result of two different computational approaches to the problem. However, now that new computational methods and technologies have been developed, this problem may be reinvestigated to fully understand the true impact of tides on submoon stability.

Though not a lot of work has been done on submoons, a good basis has been laid for future work. One of the most recent submoon studies by Kollmeier & Raymond (2019) provides a succinct overview of the current knowledge on submoon stability shown in Figure 6 (Fig. 1 of Kollmeier & Raymond). This figure summarizes theoretical submoon stability zones around the moons of planets in our own Solar system. For each planet, the moons are shown as black circles on a grid of orbital distances versus moon radius. The stability zones in this space are then mapped out for submoons of various size. The dotted line represents submoons with a radius of five kilometers, the solid line represents a radius of ten kilometers, and the dashed line represents twenty kilometers. As the orbital distance and radius of the moon increase, so does the stability probability of the submoons. In addition,

larger submoons generally have smaller stability regions than small submoons [31]. These findings are extensions of the work of Reid (1973) and Conway (1985) and agree with their results.

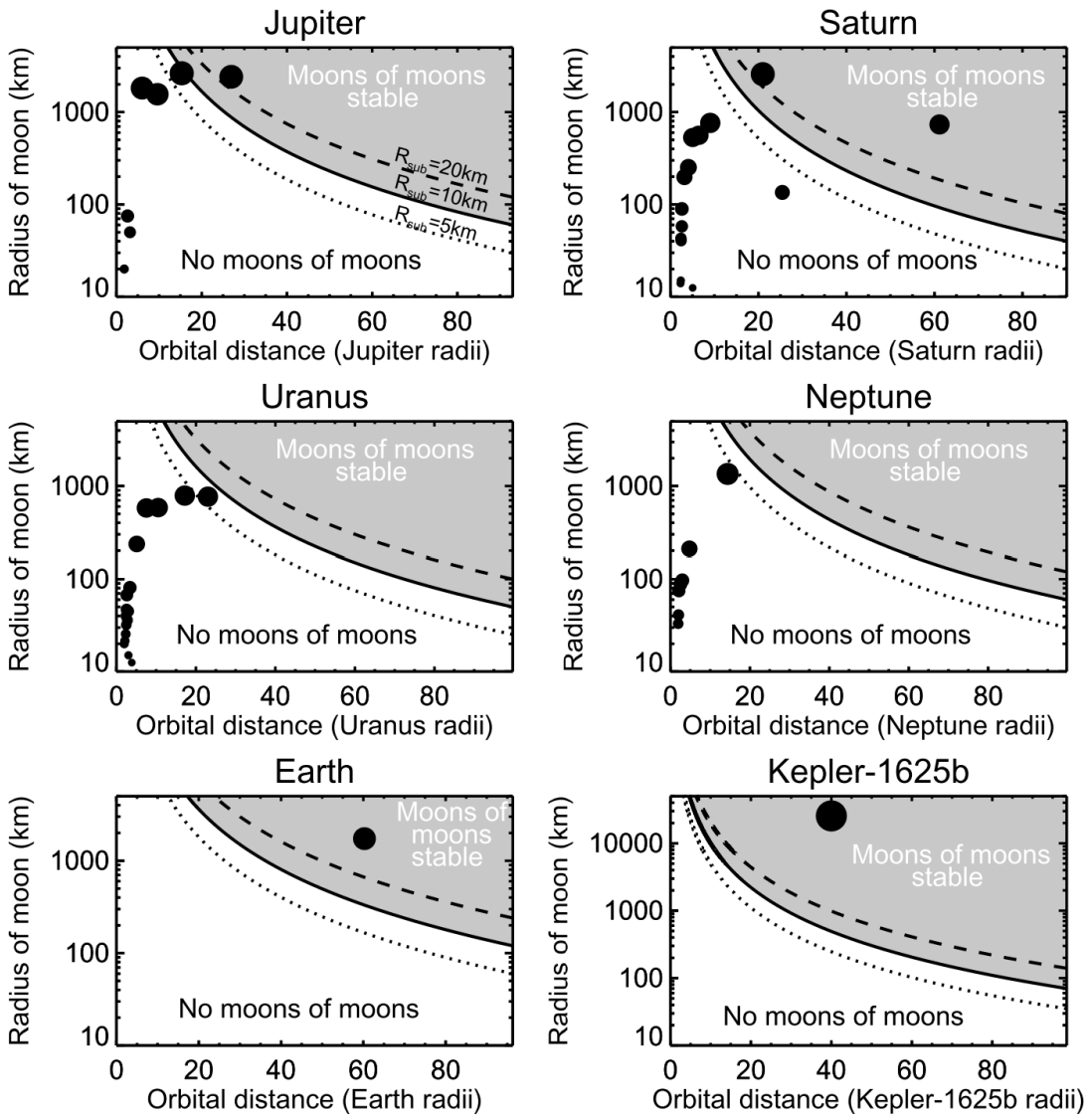

Figure 6: This figure from Figure 1 of Kollmeier & Raymond (2019) shows the stability regions of submoons around the outer planets of the Solar system, along with Earth and Kepler-1625b, as a function of orbital distance and radius of the moon. The gray area indicates the region in the parameter space where submoons with a radius of ten kilometers are stable for at least the age of the Solar system. In addition, the dashed line shows the border of the stability region for twenty kilometer submoons while the dotted line shows the border for five kilometer submoons. The moons of each planet are plotted within this parameter space as well [31].

Overall, though some early work has been done to investigate the factors affecting submoon stability, there is much more left to uncover. Many mechanisms and phenomena have

yet to be accounted for in theoretical or computational models. For example, the effects of neighboring bodies including perturbations from the star and planet, perturbations from neighboring planets, and forces from additional moons have yet to be modeled. Additionally, the properties of the submoon such as inclination, eccentricity, and pro- and retrograde orbits have not been considered. Furthermore, because a submoon orbits a moon, the motion of that moon due to tidal forces must also affect the submoon. Lastly, most existing submoon studies have focused on short time scales, and more research is needed to investigate long-term stability.

Many of these open questions about submoons require simulations that take many factors into account at once, including gravitational forces from the star, planet, and any additional moons. This can be accomplished using an N-Body code that accounts for all bodies in the system and their interactions over time.

2 Computational Methods for Studying Submoon Stability

2.1 N-Body Legacy Code

In order to simulate a possible submoon system, a Fortran N-Body code was used. This legacy code calculates the equations of motion for each body in the system as well as the forces between bodies. The original two- dimensional code was developed by Craig Agnor at the Miami University, Ohio in 1996 and was based on the Hermite Integrator with Individual Timestep Scheme (HITS) algorithm. The code was consequently improved as a third dimension was added by Himburg (1998) and gas drag was added by Bullard (1999). The code was also extended to include asteroids, rigid body rotation, and planetary satellites (Abel 2001; Carpenter 2001; Fuse 2002).

For each initialized body, the code designates a time (t_i), timestep (Δt_i), position (X_i), velocity (v_i), acceleration (a_i), and jerk ($\frac{d\vec{a_i}}{dt}$). The equations of motion for the bodies are then calculated over a series of iterative steps. First, the calculations are advanced to the first relevant time. This is done by selecting the particle with the smallest value of $t_i + \Delta t_i$ is selected and setting the global time within the code, t, to this value. The predicted positions and velocities of all the particles are then calculated at this time t. This is accomplished through third order Taylor expansions given by

$$\vec{X_{p,j}} = \frac{(t-t_j)^3}{6}\frac{d\vec{a_j}}{dt} + \frac{(t-t_j)^2}{2}\vec{a_j} + (t-t_j)\,\vec{v_j} + \vec{X_j}, \tag{7}$$

where $\vec{X_{p,j}}$ is the predicted position of particle j which had a position of $\vec{X_j}$, a velocity of $\vec{v_j}$, an acceleration of $\vec{a_j}$, and a jerk of $\frac{d\vec{a_j}}{dt}$ at time t_j, and

$$\vec{v_{p,j}} = \frac{(t-t_j)^2}{2}\frac{d\vec{a_j}}{dt} + (t-t_j)\,\vec{a_j} + \vec{v_j}, \tag{8}$$

where $\vec{v_{p,j}}$ is the predicted velocity of particle j which had a velocity of $\vec{v_j}$, an acceleration of $\vec{a_j}$, and a jerk of $\frac{d\vec{a_j}}{dt}$ at time t_j. The index j is run through all particles in the simulation. Using these predicted values for position and velocity at time t, the acceleration and jerk are then calculated. The acceleration of each body due to gravitational forces is found by summing the gravitational interactions between each object as given by

$$\vec{a_i} = \sum_{j\neq i}[\frac{Gm_j\vec{r_{ij}}}{r_{ij}^3}], \tag{9}$$

where G is the gravitational constant, m_j is the mass of an object, and $\vec{r_{ij}}$ is the distance between the i^{th} and the j^{th} objects defined by $\vec{r_{ij}} = \vec{X_{p,j}} - \vec{X_{p,i}}$. Correspondingly, the jerk, which is defined as the instantaneous change in acceleration, is calculated via the derivative

of the acceleration and can be described by

$$\frac{d\vec{a_i}}{dt} = \sum_{j \neq i} G m_j \left[\frac{\vec{v_{ij}}}{r_{ij}^3} - 3 \frac{\vec{r_{ij}} \left(\vec{v_{ij}} \cdot \vec{r_{ij}} \right)}{r_{ij}^5} \right], \tag{10}$$

where G, m_j, and $\vec{r_{ij}}$ are defined as above and $\vec{v_{ij}}$ is the relative velocity between the i^{th} and j^{th} objects given by $\vec{v_{ij}} = \vec{v_{p,j}} - \vec{v_{p,i}}$. The predicted position and velocities values are then corrected using a third order Hermit interpolation polynomial such that

$$\vec{X_i} \left(t_i + \Delta t_i \right) = \vec{X_{p,i}} + \frac{\Delta t_i^4}{24} \frac{d^2 \vec{a_{0,i}}}{dt^2} + \frac{\Delta t_i^5}{120} \frac{d^3 \vec{a_{0,i}}}{dt^3}, \tag{11}$$

where $\vec{X_i} \left(t_i + \Delta t_i \right)$ is the position of the i^{th} particle at time $(t_i + \Delta t_i)$, $\vec{a_{0,i}}$ is the acceleration of body i at the global time t, and

$$\vec{v_i} \left(t_i + \Delta t_i \right) = \vec{v_{p,i}} + \frac{\Delta t_i^3}{6} \frac{d^2 \vec{a_{0,i}}}{dt^2} + \frac{\Delta t_i^4}{24} \frac{d^3 \vec{a_{0,i}}}{dt^3}, \tag{12}$$

where all values are defined as above. The corrected acceleration of body i can be found by

$$\vec{a_i} \left(t \right) = \vec{a_{0,t}} + \Delta t \frac{d\vec{a_{0,i}}}{dt} + \frac{\Delta t^2}{2} \frac{d^2 \vec{a_{0,i}}}{dt^2} + \frac{\Delta t^3}{6} \frac{d^3 \vec{a_{0,i}}}{dt^3}, \tag{13}$$

where $\vec{a_{0,t}}$ is defined as above, $\frac{d\vec{a_{0,i}}}{dt}$ is the jerk of the body calculated at the global time, t, and $\Delta t = t - t_i$.

The second and third derivatives of the acceleration used in these corrected position, velocity, and acceleration calculations are given by

$$\frac{d^2 \vec{a_{0,i}}}{dt^2} = \frac{-6 \left(\vec{a_{0,i}} - \vec{a_{1,i}} \right) - \Delta t_i \left(4 \frac{d\vec{a_{0,i}}}{dt} + 2 \frac{d\vec{a_{1,i}}}{dt} \right)}{\Delta t_i^2}, \tag{14}$$

and

$$\frac{d^3\vec{a_{0,i}}}{dt^3} = \frac{12\left(\vec{a_{0,i}} - \vec{a_{1,i}}\right) + 6\Delta t_i\left(\frac{d\vec{a_{0,i}}}{dt} + \frac{d\vec{a_{1,i}}}{dt}\right)}{\Delta t_i^3}, \tag{15}$$

where $\vec{a_{1,i}}$ and $\frac{d\vec{a_{1,i}}}{dt}$ are the acceleration and jerk calculated at time $t_i + \Delta t$.

Once the position and velocity vectors for a particle have been corrected, the code calculates a new timestep using the acceleration and its time derivatives. This timestep calculation was developed by Aarseth (1985) and is given by

$$\sqrt{\eta\frac{|\vec{a_{1,i}}|\left|\frac{d^2\vec{a_{1,i}}}{dt^2}\right| + \left|\frac{d\vec{a_{1,i}}}{dt}\right|^2}{\left|\frac{d\vec{a_{1,i}}}{dt}\right|\left|\frac{d^3\vec{a_{1,i}}}{dt^3}\right| + |\vec{a_{1,i}}|^2}}, \tag{16}$$

where η is an adjustable parameter controlling the accuracy of the program. The acceleration and jerk are calculated directly from Equations 9 and 10, while the second derivative is given by

$$\frac{d^2\vec{a_{1,i}}}{dt^2} = \frac{d^2\vec{a_{0,i}}}{dt^2} + \Delta t_i\frac{d^3\vec{a_{0,i}}}{dt^3}, \tag{17}$$

where the derivative values are defined by Equations 14 and 15 and Δt_i is the initial timestep. The third derivative term in Equation 16 is constant due to the use of a third order interpolation where all higher derivatives are taken to be zero.

Using this new timestep for each particle, the program identifies the new smallest value of $t_i + \Delta t_i$ and the process is repeated.

This code can be used to simulate the motion of astronomical bodies such as planets, asteroids, and satellites. In addition, it has been used in the past to successfully simulate planet formation[33] and planet migration, such as Thommes model migration in which proto-Uranus and -Neptune are formed on orbits between Jupiter and Saturn and are then ejected to their current stable orbits through gravitational resonances [34].

2.2 Data Analysis Codes

The output of the planet formation code includes information about collisions within the system, the energy of the bodies, and the initial orbital parameters of the objects including mass, density, radius, semi-major axis, eccentricity, and inclination. In addition, the code outputs the three-dimensional positions and velocities of each body for each time step. This data, while useful can be difficult to sift through, so two different analysis codes are used to extract useful values from the given data: one for planets and one for moons.

The planet data analysis code reads the Cartesian velocity and position values of each object and converts these values to ecliptic coordinates. Its outputs include the mass, semi-major axis, eccentricity, and inclination of each individual body at a certain, user-defined, time. These ecliptic coordinates allow for easier analysis of the data through the comparison of semi-major axes, eccentricities, and inclinations for different bodies and over time.

The cartesian to ecliptic conversion is done using the solutions to Kepler's equations outlined in Danby (1988) [32]. Kepler's equation, given by

$$M = E - e\sin E, \tag{18}$$

describes the motion of a body on an elliptic orbit, where M is the mean anomaly, E is the eccentric anomaly, and e is the eccentricity of the orbit. The mean anomaly, M, describes the angular distance from the pericenter at time t and is given by

$$M = n\,(t - T)\,, \tag{19}$$

where n is the mean angular motion of the body and T is the time at which the body is at the pericenter. The eccentric anomaly, E, also describes the angular position of the body

along its orbit and is defined by

$$r = a\,(1 - e\cos E)\,, \tag{20}$$

where r is the distance from the focus to the body, a is the semi-major axis of the ellipse, and e is again the eccentricity [32]. From Equations 18, 19, and 20, the cartesian coordinates of the body with the origin at the attracting focus of the ellipse are given by

$$X = a\,(cosE - e)\,, \tag{21}$$

$$Y = a\sqrt{1 - e^2}sinE, \tag{22}$$

$$\dot{X} = -\frac{na^2}{r}\mathrm{sinE}, \tag{23}$$

and

$$\dot{Y} = \frac{na^2\sqrt{1 - e^2}}{r}\mathrm{cosE}, \tag{24}$$

where the variables are as defined above [32]. These relations are thus used in the planet analysis code to convert from cartesian to ecliptic coordinates.

The moon data analysis code is very similar in structure and function to the planetary analysis code. It works using the same method, but finds the ecliptic coordinates of moons in relation to a user-defined mother planet rather than in relation to the Sun.

2.3 Additions to the Code

In order to simulate submoons, a subroutine was added to the existing planet formation code. First, the option to call this subroutine and introduce a submoon into the system was added to the main body of the code. This was done using a switch and an If-Then statement. It was specified that the submoon could only be added if a moon was also added

to the simulation. Within this If-Then statement, the user can specify around which planet and moon the submoon should orbit, if there are multiple bodies in the simulation.

The submoon subroutine itself was based heavily on the existing moon subroutine, which places a moon around a user-specified planet. It was, however, changed to account for the submoons orbit around a moon instead of a planet and required data about the host moon's mass and heliocentric coordinates in addition to those of the planet.

The subroutine places bodies with user-specified characteristics such as mass, density, eccentricity, inclination, and radius around the nth body in the simulation at a given semi-major axis. The initial ecliptic coordinates are then converted to heliocentric coordinates so that they are in the same coordinate system as the other bodies in the simulation. This is accomplished first through the addition of a new subroutine which reverses the cartesian to ecliptic calculation described above to convert the positions and velocities of submoons from ecliptic to Cartesian coordinates. The resulting Cartesian coordinates of the submoon are relative to the parent moon, so the heliocentric parent moon positions and velocities are added in order to describe the location of the submoon relative to the Sun. This body is then introduced into the system and the process described in Subsection 2.1 continues.

A submoon data analysis code was also created to convert the Cartesian output of the main planet formation code to moon-centric ecliptic coordinates. This code uses the same methods described for the planet and moon data analysis codes, calculating relative to a user-defined moon rather than relative to a planet or the Sun. Though the methods for converting between Cartesian and ecliptic coordinates described earlier are based on a two-body system, they must still be used for the three-body system, simply because the three-body system is infinitely more complex and has no 'easy' solutions. However, due to the fact that the majority of the forces acting on the submoon stem from the moon and the large number of trials that are conducted in any study, the effects of this discrepancy become negligible.

3 Results

3.1 Earth, Moon, Satellite System

Because there are no known submoons, the new submoon subroutine was tested by placing a fictional submoon around the Earth's moon. This submoon body is based loosely on the Explorer 35 lunar satellite, which orbited the moon for a short period of time [35, 36]. The three bodies initialized in this test code were the Earth, its Moon, and the Lunar satelite (EMS). The orbital and physical parameters are summarized in Table 2.

	Planet	**Moon**	**Submoon**
Mass [kg]	3.9736×10^{24}	7.349×10^{22}	104.3
Density [kg/m^3]	5.515×10^{3}	3.34×10^{3}	2.0×10^{3}
Semi-major Axis [m]	1.49598×10^{11}	3.844×10^{8}	5.0×10^{6}
Eccentricity	0.01671022	0.0549	0.0136973
Inclination [radians]	8.72665×10^{-7}	8.9884×10^{-2}	0.04487

Table 2: This table shows the orbital and physical parameters of the intialized bodies for the first set of trials. The planetary characteristics were based on the Earth, while the moon characteristics were based on the Moon. The submoons characteristics were based loosely on past lunar satellites. The semi-major axis listed for each body is given relative to its host.

Once the code was running and the output values seemed reasonable, the actual behavior of the planet, moon, and submoon over time was investigated for the configuration of bodies described by Table 2.

Initially, the simulations were run for 10,000 years, with a timestep of 500 years, meaning that the values for each body were updated every 500 years. These simulations showed that both the moon and the planet were on stable orbits around the Sun, but the behavior of

the submoon was scattered. This can be seen in Figure 7, where the blue and green points represent the planet and moon, respectively, while the red points show the submoon's x and y positions. In addition, Figure 8 shows the motion of the submoon relative to its host moon. The submoon could be in orbit around the moon, though there are not enough data points to clearly identify a trend. In addition, its motion relative to the Sun indicates that it might be in orbit around the star rather than the moon. This could indicate a problem with the code or merely and unstable submoon.

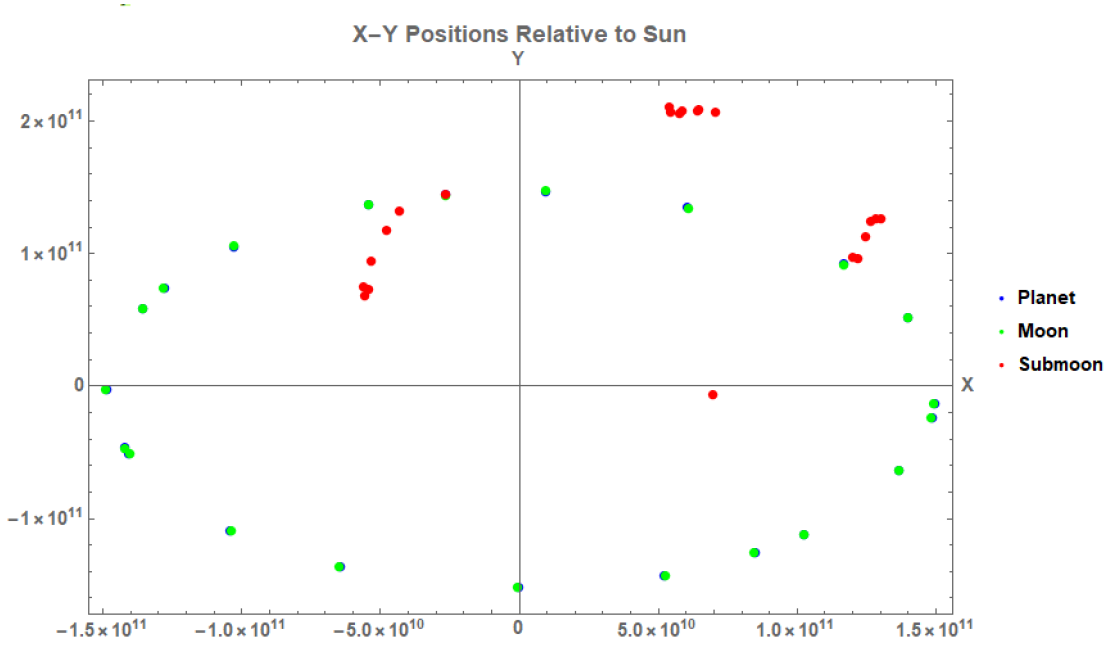

Figure 7: This figure shows the positions of the planet, moon, and submoon with the characteristics given in Table 2 in the x-y plane relative to the Sun. The simulation was run to 10,000 years with a timestep of 500 years. The blue, green, and red points correspond to the planet, moon, and submoon respectively.

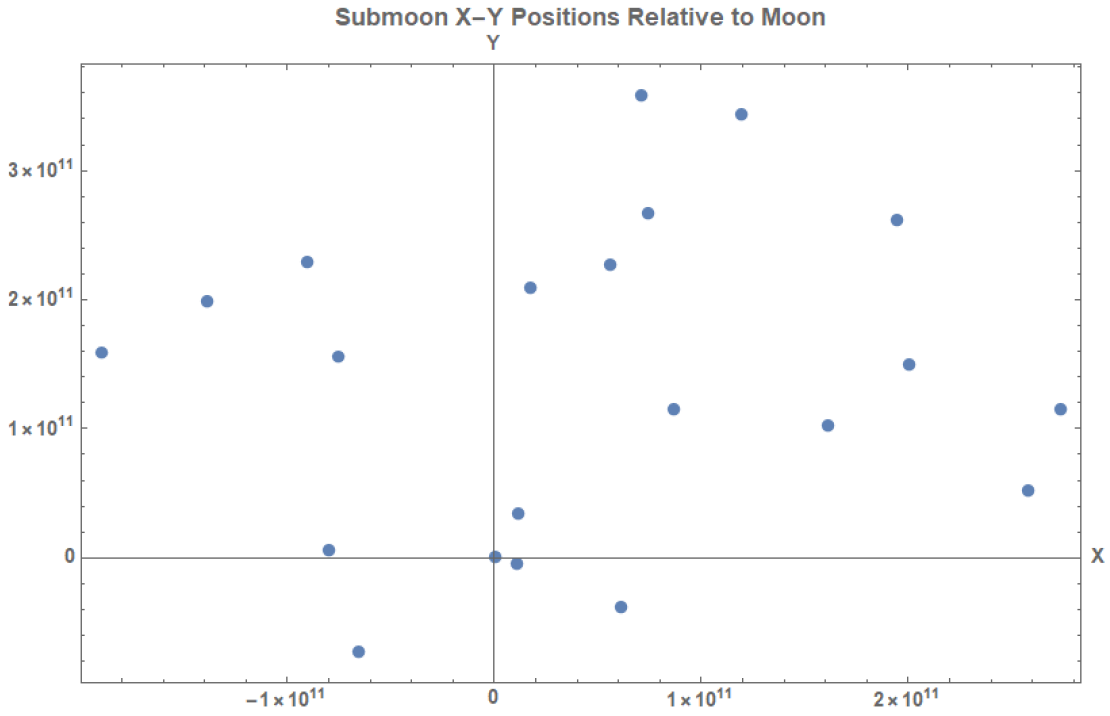

Figure 8: This figure shows the positions of the submoon with the characteristics given in Table 2 in the x-y plane relative to the Moon. The simulation was run to 10,000 years with a timestep of 500 years.

Because the submoon data did not seem to show the whole picture, additional simulations were run, again for 10,000 years but with a timestep of 50 years instead of 500. These revealed a much clearer picture of the submoon's motion around the Sun, shown in Figure 11. The submoon appears to orbit the Sun instead of the moon, as intended. However, Figure 10, which shows the path of the submoon around the moon, seems to indicate the submoon may in fact be orbiting the moon at a large semi-major axis. Once again, the data for the submoon is relatively sparse, and more points are necessary to fully capture the submoon's motion.

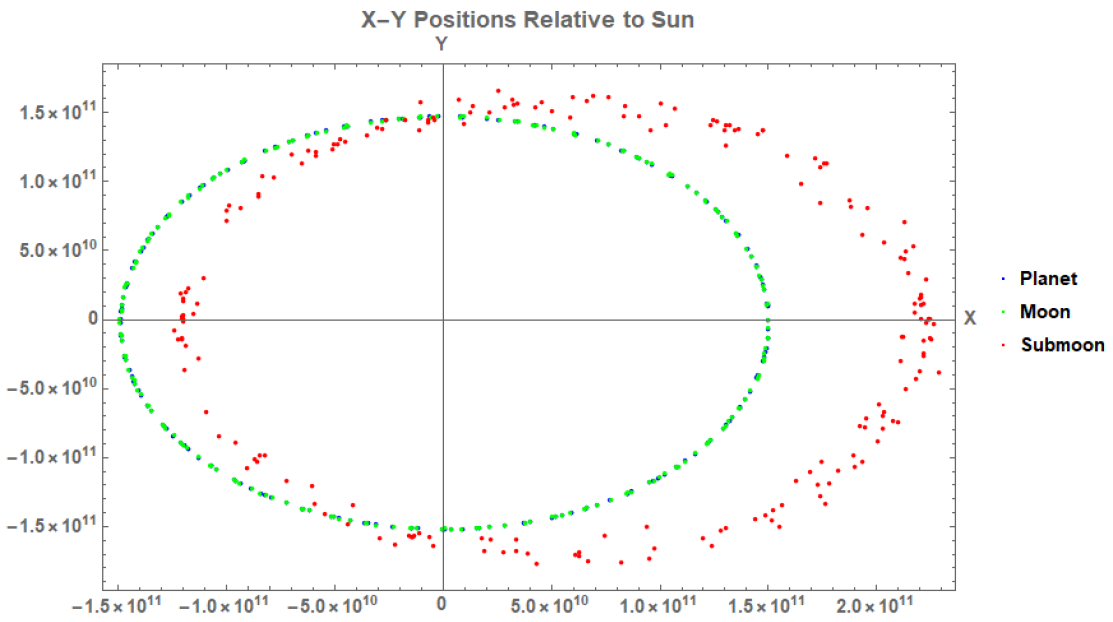

Figure 9: This figure shows the positions of the planet, moon, and submoon with the characteristics given in Table 2 in the x-y plane relative to the Sun. The simulation was run to 10,000 years with a timestep of 50 years. The blue, green, and red points correspond to the planet, moon, and submoon respectively.

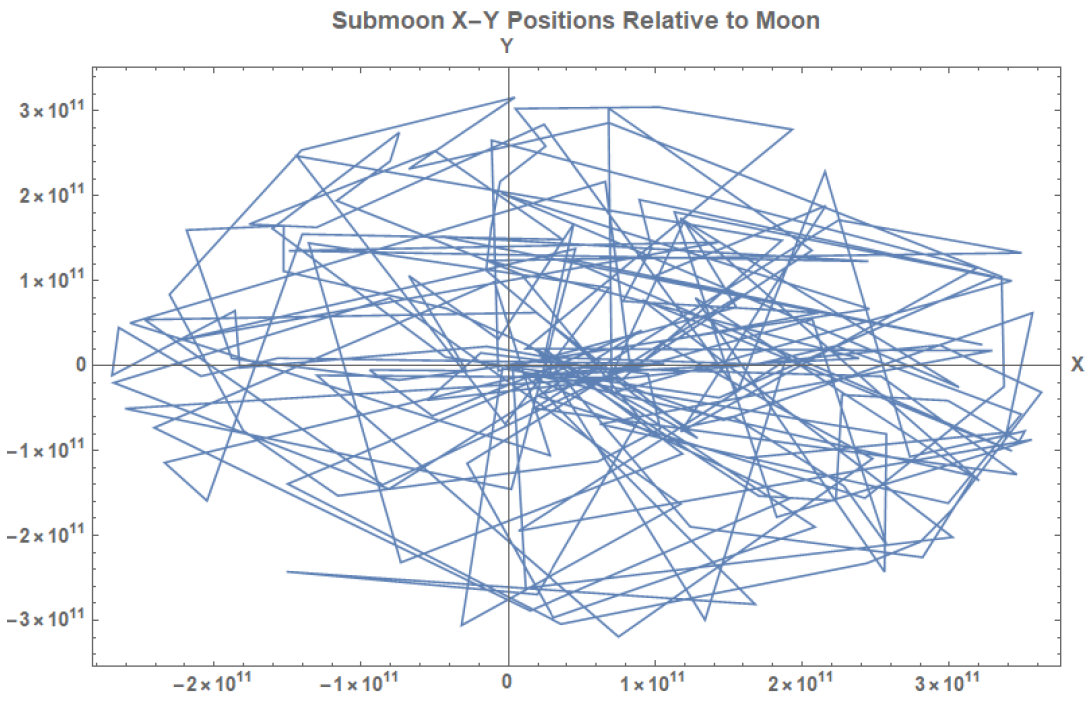

Figure 10: This figure shows the positions of the submoon with the characteristics given in Table 2 in the x-y plane relative to the Moon. The simulation was run to 10,000 years with a timestep of 50 years.

Thus, the timestep was again decreased from 50 years to five years, though the total simulation time was kept at 10,000 years. The results of these further simulations are shown in Figures 11 and 10. Figure 11 visualizes the motion of the planet, moon, and submoon around the Sun. The submoon in red seems to orbit the Sun on a wide, elliptical orbit with a relatively large variation in semi-major axis. Figure 10 shows the progression of the submoon's motion around the Moon over time. It is clear that the submoon is not orbiting the moon directly. Once again, this result may be due to a problem with the code, but it may also be the result of a very unstable submoon that is quickly removed from orbit around the moon, only to be caught in an orbit around the Sun.

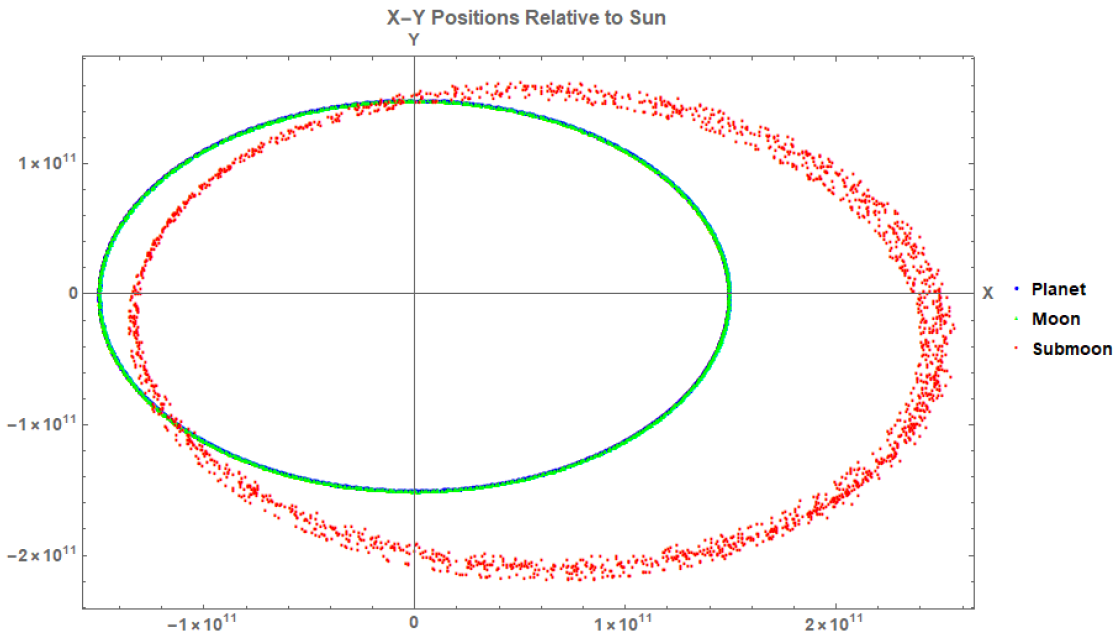

Figure 11: This figure shows the positions of the planet, moon, and submoon with the characteristics given in Table 2 in the x-y plane relative to the Sun. The simulation was run to 10,000 years with a timestep of 5 years. The blue, green, and red points correspond to the planet, moon, and submoon respectively.

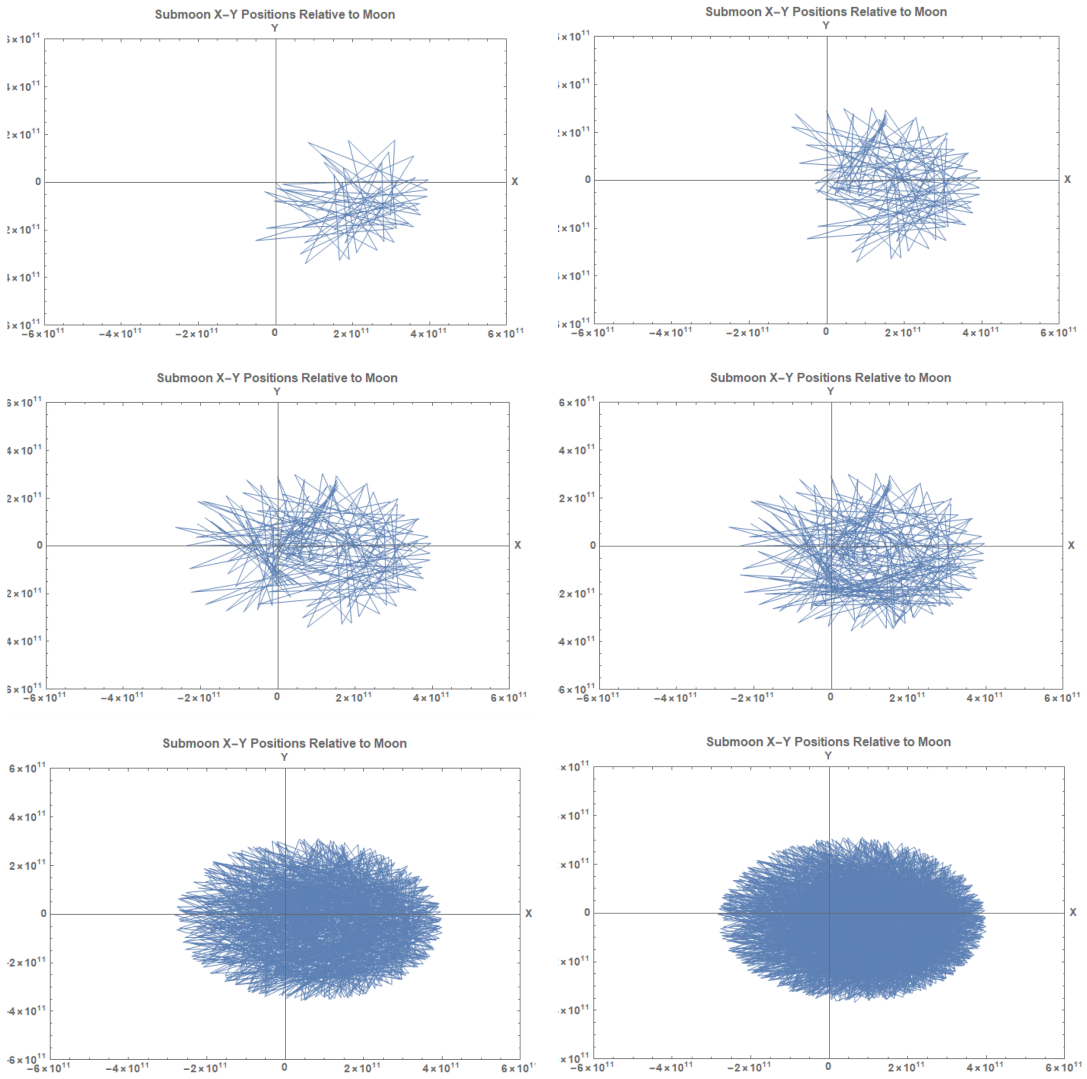

Figure 12: This figure shows the positions of the submoon with the characteristics given in Table 2 in the x-y plane as a function of position relative to the Moon. The simulation was run to 10,000 years with a timestep of 50 years. The first plot includes the first 50 points of the simulation. The remaining plots include the first 100, 150, 200, 1000, and 2000 points to show the evolution of the orbit over time.

In order to more closely investigate the behavior of the submoon when it is first placed into orbit around the moon, a further set of simulations was run, this time with a maximum run time of 100 years, and a 0.01 year timestep. These changes allowed for a detailed look at the behavior of the submoon early on. The results in the x-y plane are summarized in

Figures 13 and 14. Relative to the Sun, the submoon continues to have what appears to be a very elliptical orbit around the star. However, when its position is viewed relative to the Moon, it becomes clear that the submoon does in fact orbit the moon, on an orbit that varies from close to wide. This orbital motion early on, along with the results from the longer simulation, indicates that the submoon was indeed placed where it was meant to be, but that its orbit around the Moon was unstable and eventually decayed until the submoon was caught in orbit around the planet. Of course, these are merely the results of a very small number of simulations, so the behavior of the submoon in this code should definitely be tested further to ensure the results are repeatable.

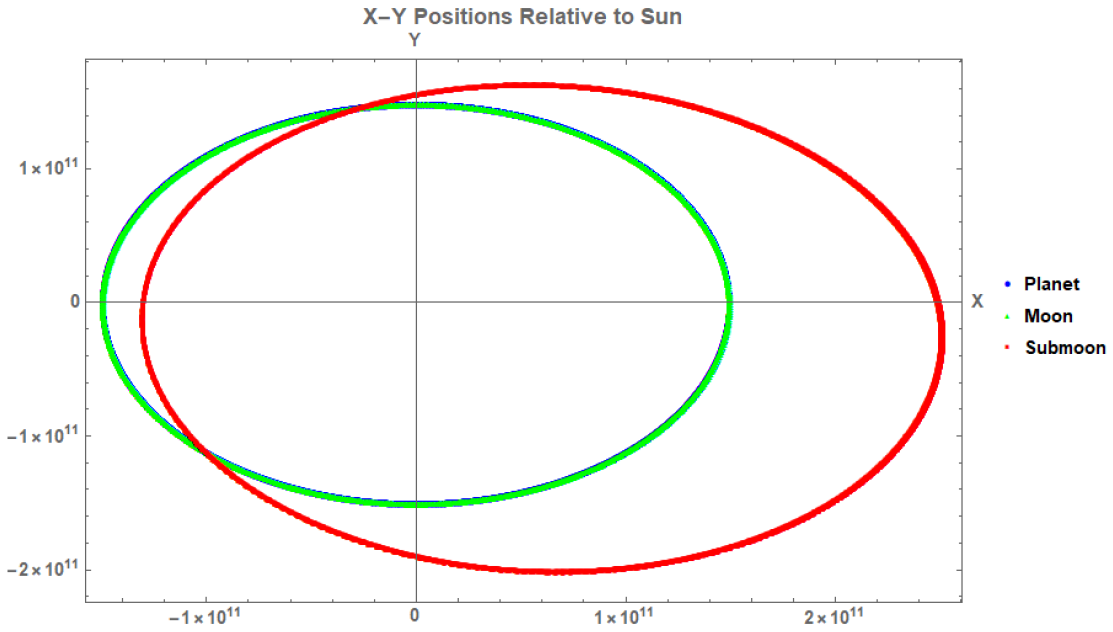

Figure 13: This figure shows the positions of the planet, moon, and submoon with the characteristics given in Table 2 in the x-y plane relative to the Sun. The simulation was run to 100 years with a timestep of 0.01 years. The blue, green, and red points correspond to the planet, moon, and submoon respectively.

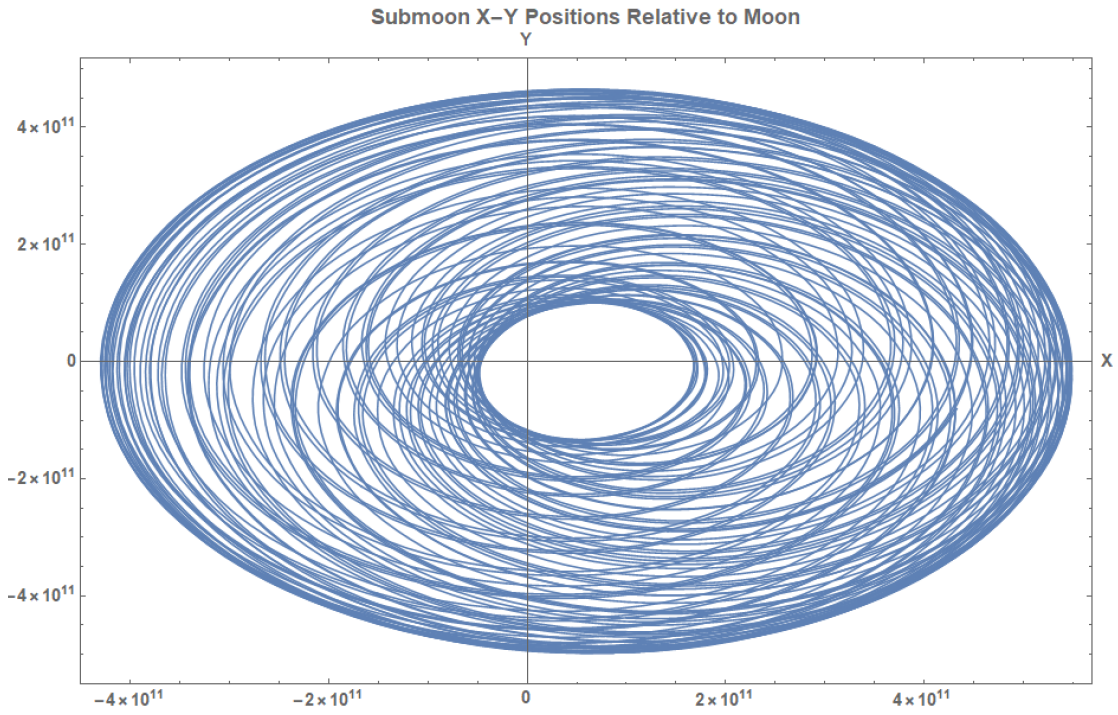

Figure 14: This figure shows the positions of the submoon with the characteristics given in Table 2 in the x-y plane relative to the Moon. The simulation was run to 100 years with a timestep of 0.01 years.

Thus far, only the submoon's motion in the x-y plane has been considered. However, its orbit is not completely flat, as seen in Figures 15 and 16. Figure 15 shows the positions of the submoon in the x, y, and z directions relative to the Sun. The submoon traces out a smooth disk, which could be expected based on the x-y motion shown in Figure 13. Interestingly, the three-dimensional motion of the submoon relative to the moon shown in Figure 16 is much less smooth. Though the orbit has a similar disk-like shape, which agrees with its x-y motion in Figure 14, the disk is significantly less smooth. These variations in smoothness are likely due to perturbations from the moon and planet and may correspond to oscillations in the semi-major axis seen in Figure 14.

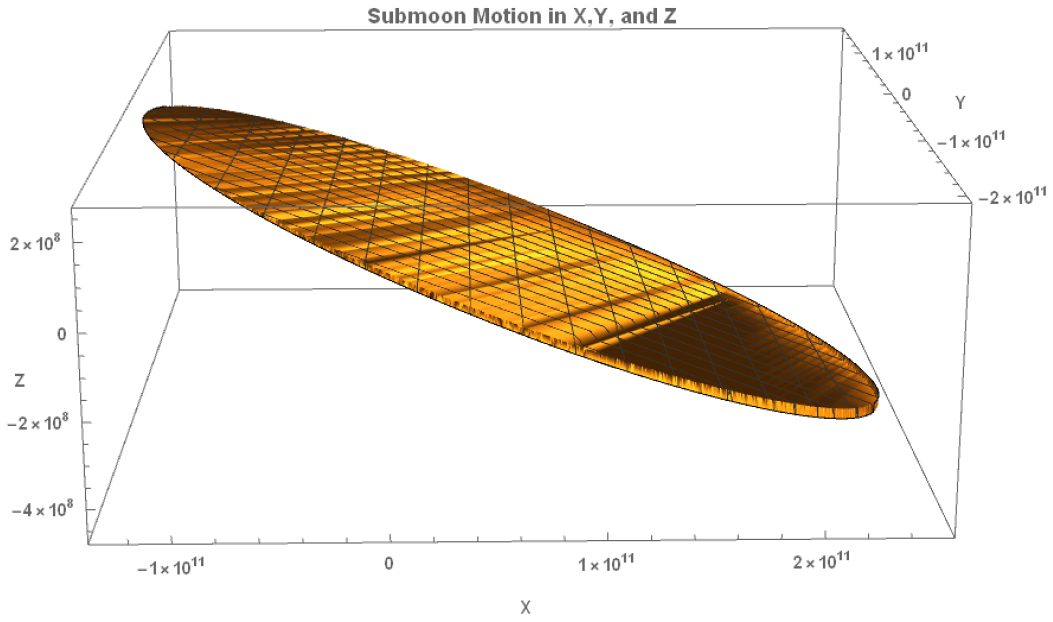

Figure 15: This figure shows the positions of the submoon with the characteristics given in Table 2 in x, y, and z relative to the Sun. The simulation was run to 100 years with a timestep of 0.01 years.

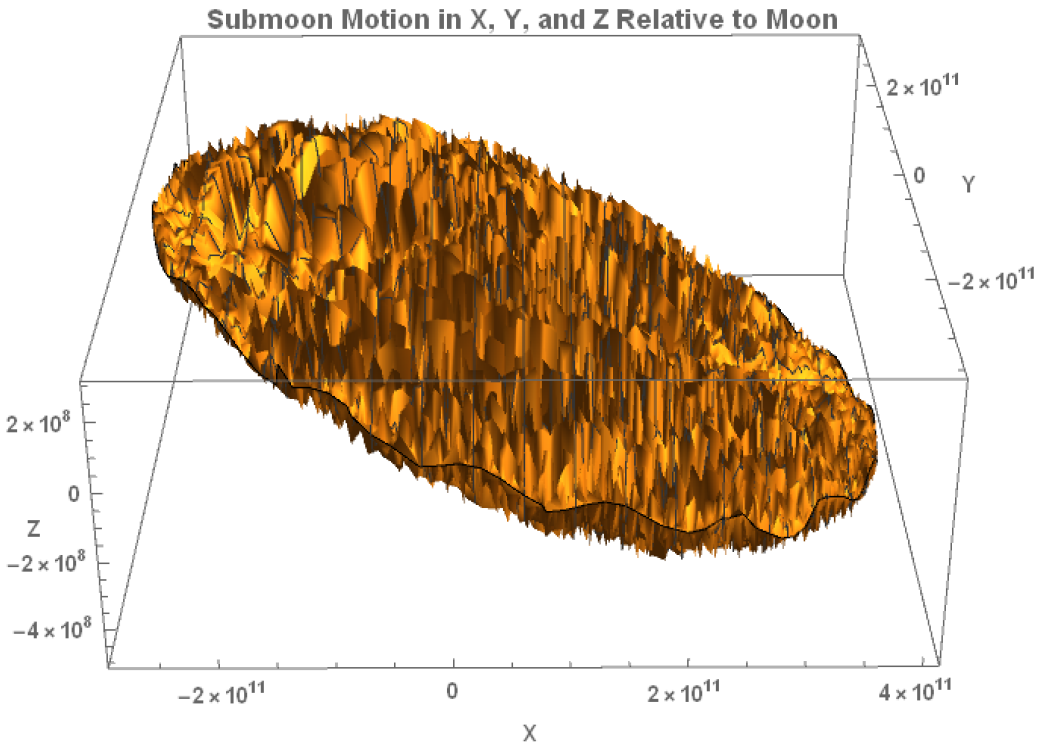

Figure 16: This figure shows the positions of the submoon with the characteristics given in Table 2 in x, y, and z relative to the Moon. The simulation was run to 100 years with a timestep of 0.01 years.

3.2 Kepler 1625bi System

Once it was established that the new submoon subroutine could place submoons on a given initial orbit and track their motion over time, a short test was done for the Kepler 1625-bi system. The initial conditions and orbital parameters for the star, planet, moon, and submoon used are summarized in Table 3. The values for the star, planet, and moon were taken directly from the models of the system published in Teachey et al. (2018) [11], while the physical and orbital characteristics of Triton, Neptune's largest moon, were used for the submoon. This configuration is referred to as the Triton configuration.

Star			
Mass [M_{Sun}]	1.0414	**Radius [R_{Sun}]**	1.73
	Planet	**Moon**	**Submoon**
Mass [kg]	6.06357×10^{27}	5.653495×10^{26}	2.1408×10^{22}
Density [kg/m^3]	3.76575×10^{3}	8.04709×10^{3}	2.059×10^{3}
Semi-major Axis [m]	1.4661×10^{11}	2.98112×10^{9}	3.548×10^{8}
Eccentricity	0.0	0.0	0.0
Inclination [radians]	0.0	0.0	2.7378

Table 3: This table shows the orbital and physical parameters of the intialized bodies for the second set of trials. The characteristics of the star, planet, and moon were based on models of the system published by Teachey et al. (2018) [11]. The submoons characteristics were based on Triton, Neptune's largest moon. The semi-major axis listed for each body is given relative to its host.

First, a trial was run with a total time of 10,000 years and a five year timestep. This trial showed that both the planet and theorized moon are stable in the given configuration for at least 10,000 years. However, on this timescale, the Triton-sized submoon was clearly not stable in orbit around the moon or even the star. This can be seen in Figures 17 and 18, which again show the motion of the submoon in the x-y plane relative to the star and moon, respectively. In the top right corner of the graph, it can be seen that the submoon moved in the vicinity of the planet and/or moon for some time before being kicked out of the system entirely. Thus, an additional trial was started to investigate the behavior of the submoon at early times.

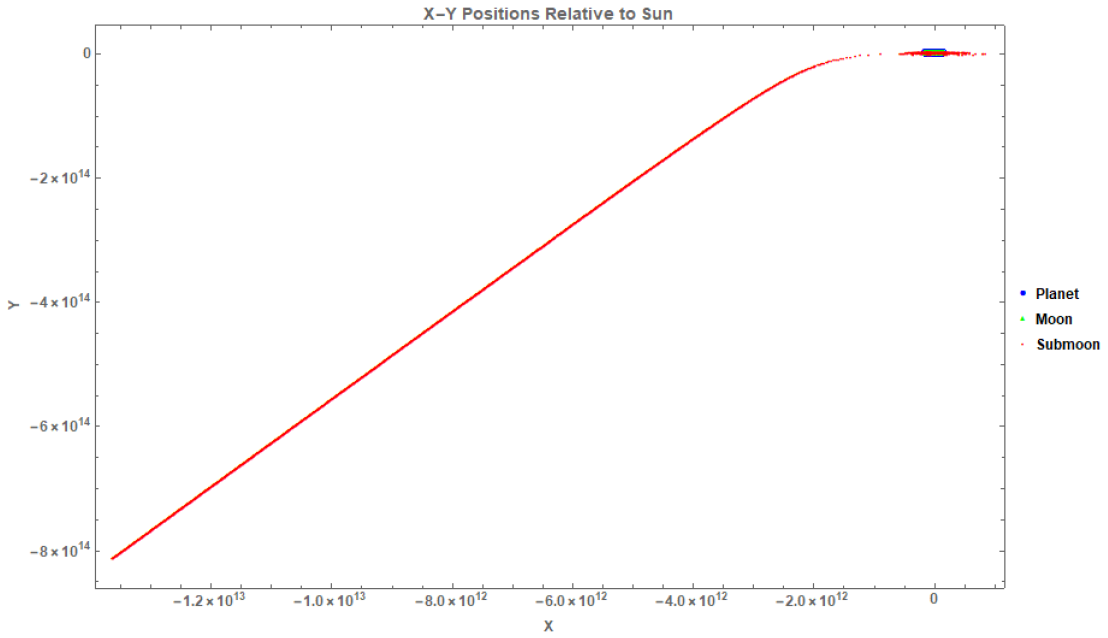

Figure 17: This figure shows the positions of the planet, moon, and submoon with the characteristics given in Table 3 in the x-y plane relative to the star. The simulation was run to 10,000 years with a timestep of 5 years. The blue, green, and red points correspond to the planet, moon, and submoon respectively. The planet and moon can be seen in the top right corner of the plot, though the submoon's rotation, in red, clearly shows that it was ejected from orbit around any of the bodies.

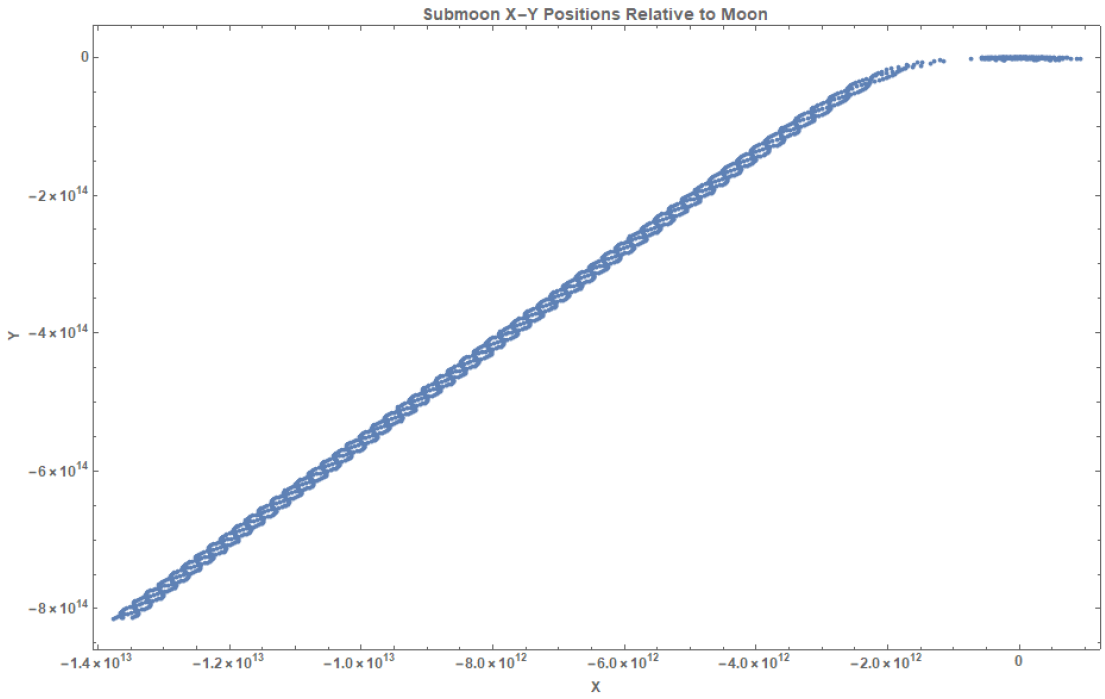

Figure 18: This figure shows the positions of the submoon with the characteristics given in Table 3 in the x-y plane relative to the moon. The simulation was run to 10,000 years with a timestep of 5 years. The submoon was clearly ejected from orbit around the moon.

The second trial had a total time of 100 years and a timestep of 0.01 years. The results are shown in Figures 19, 20, 21, and 22. Figure 19 shows the precession of the submoon's orbit relative to the star. It may indicate either a very wide, unstable orbit around the moon, or an unstable orbit purely around the star. However, Figure 20 shows the motion of the submoon around the moon. The orbit is highly variable and not circular, despite the fact that the submoon was initialized on a completely circular orbit with an eccentricity of 0.0. However, the body does appear to orbit around the moon, at least on a very short timescale. Interestingly, plots of the three-dimensional submoon orbit both relative to the star (Fig. 21) and relative to the moon (Fig. 22), show a flat area and a highly distorted area. In both cases, this phenomenon is likely the product of the submoon's elliptical orbit. When it is far from the other bodies in the system, its orbit become smooth and flat, while it becomes more chaotic and distorted when the submoon experiences gravitational perturbations from

the moon and planet.

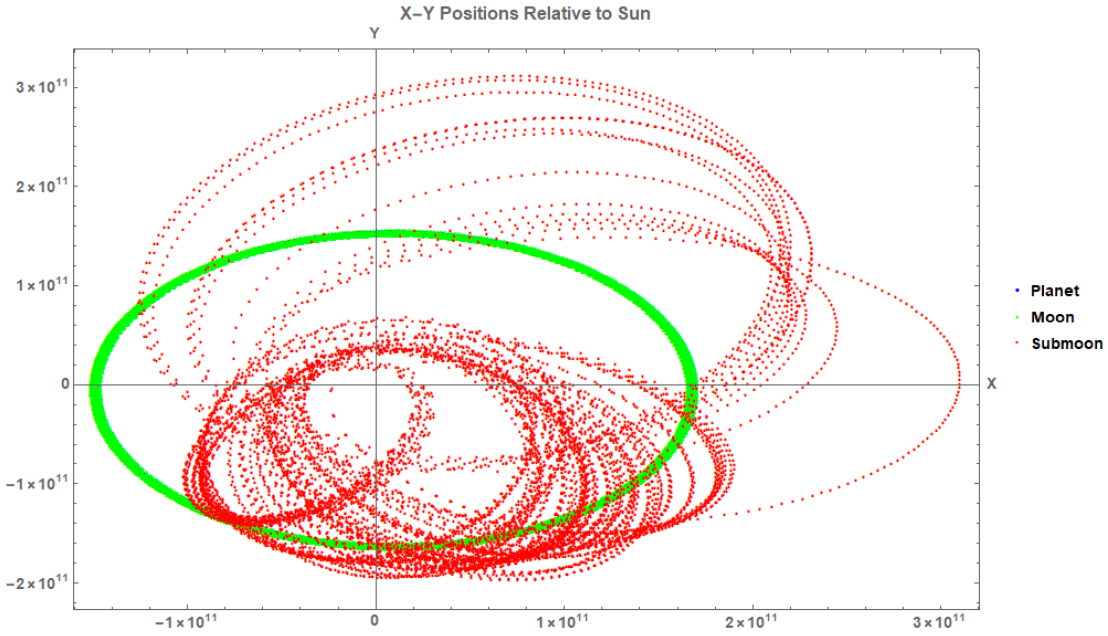

Figure 19: This figure shows the positions of the planet, moon, and submoon with the characteristics given in Table 3 in the x-y plane relative to the star. The simulation was run to 100 years with a timestep of 0.01 years. The blue, green, and red points correspond to the planet, moon, and submoon respectively. The submoon is in a quickly precessing unstable orbit around the star.

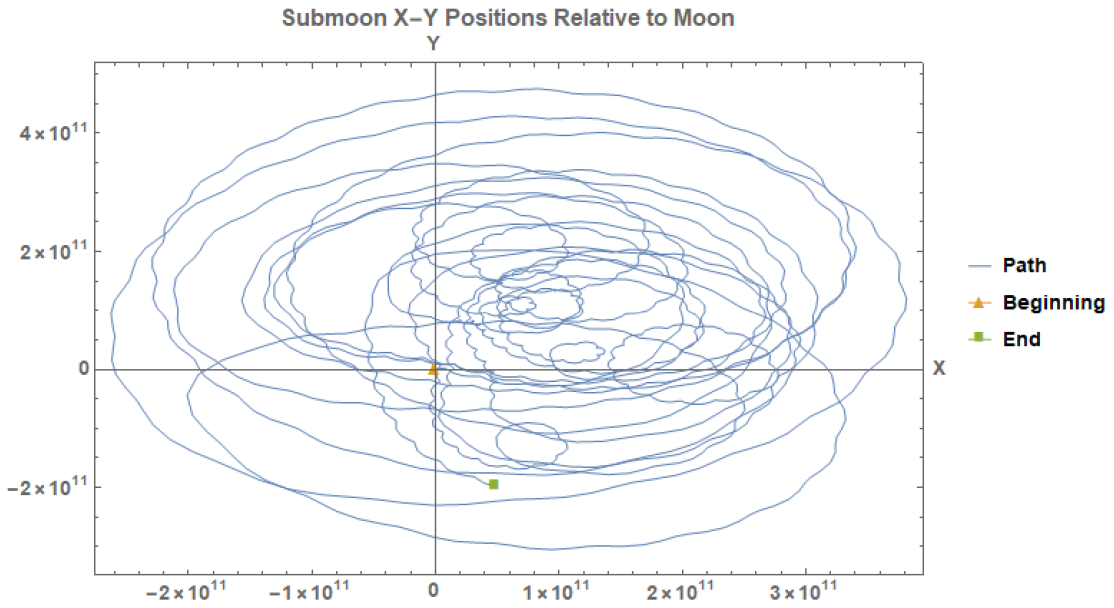

Figure 20: This figure shows the positions of the submoon with the characteristics given in Table 3 in the x-y plane relative to the moon. The simulation was run to 100 years with a timestep of 0.01 years. The orange triangle shows the submoon's initial position, while the green square shows its final position after 100 years. Though the submoon is not in a stable orbit around the moon, it is also not ejected from the system after 100 years.

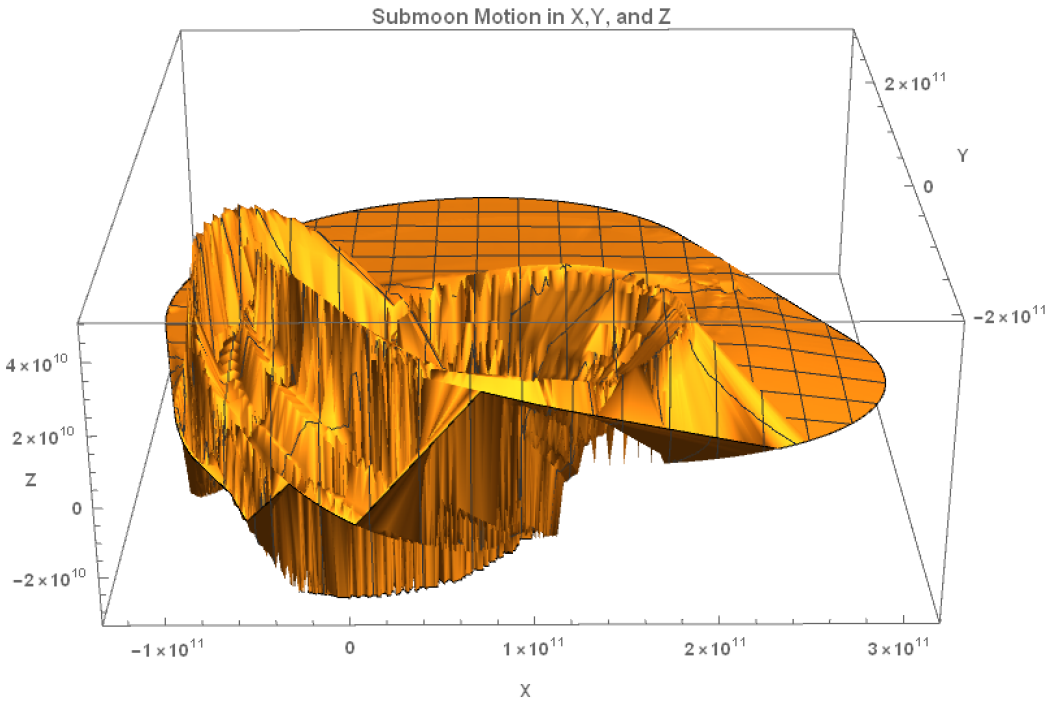

Figure 21: This figure shows the positions of the submoon with the characteristics given in Table 3 in x, y, and z relative to the star. The simulation was run to 100 years with a timestep of 0.01 years. The distortion in the bottom left corner is likely due to strong interactions between the star, planet, moon, and submoon when the submoon approaches the star.

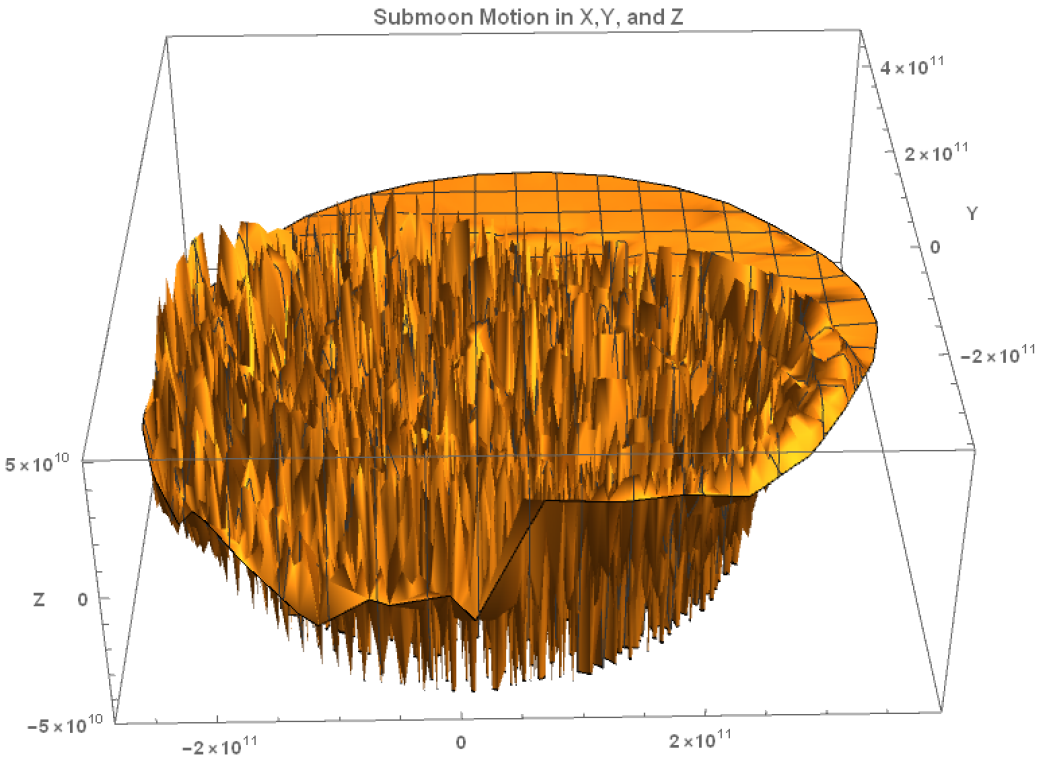

Figure 22: This figure shows the positions of the submoon with the characteristics given in Table 3 in x, y, and z relative to the moon. The simulation was run to 100 years with a timestep of 0.01 years. Once again, the distortion in the lower left corner is likely a product of strong gravitational forces acting on the submoon as it approaches both the moon and planet.

Kollmeier & Raymond (2019) found the upper boundary on the mass of a stable submoon orbiting Kepler 1625-bi based on the tidal evolution of the system to be approximately the mass of the dwarf planet Ceres [31]. Thus, another set of trials was run in which the submoon's mass and density were adjusted to approximate those of Ceres as shown in Table 4. The semi-major axis was also decreased to 3.5×10^8 meters. This set of parameters is referred to as the Ceres configuration.

Ceres-sized Submoon	
Mass [kg]	9.47×10^{20}
Density [kg/m3]	2.09×10^{3}

Table 4: This table shows the orbital and physical parameters of the Ceres-like submoon. The planet and star characteristics described in Table 3 are not changed for this set of trials. The submoons characteristics, however, were based on Ceres, a small dwarf planet [37]. The semi-major axis listed is relative to the moon.

Three different simulations were run with these parameters, each initializing the submoon at a different, randomly determined location along its orbit. They were run for 100 years with a timestep of 0.01 years. In the first case, shown in Figure 23, the submoon was initially caught in wide, precessing orbit around the star. After 75.65 years, it collided with and merged into the star. In the second case, the submoon was quickly removed from the system and was not caught in orbit around any of the bodies, as shown in Figure 24. Finally, in the third case, the submoon immediately crashed into the planet. Thus, even with a smaller mass, the submoon was still not stable.

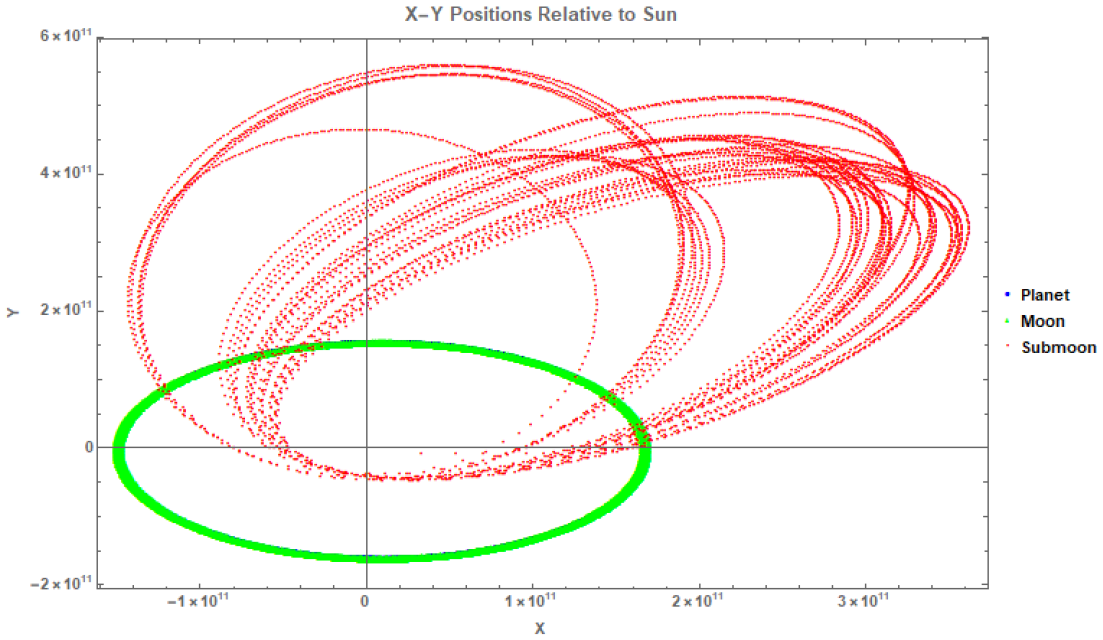

Figure 23: This figure shows the positions of the planet, moon, and submoon with the characteristics given in Table 3 in the x-y plane relative to the star. The simulation was run to 100 years with a timestep of 0.01 years. The blue, green, and red points correspond to the planet, moon, and submoon respectively. The submoon is in a quickly precessing unstable orbit around the star until it collides with the star after 75.65 years.

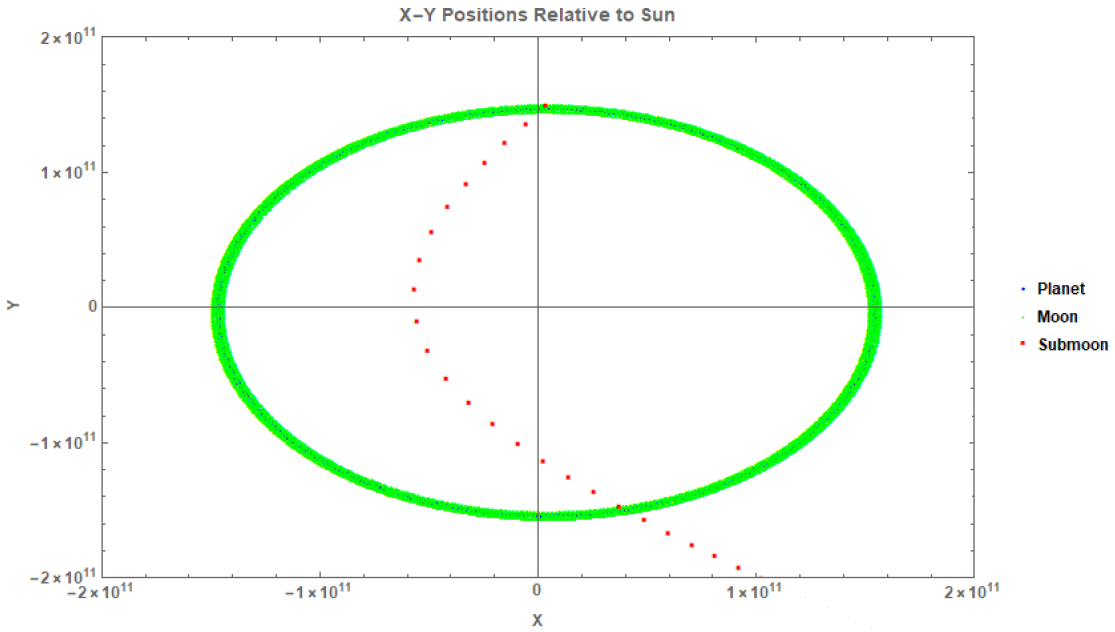

Figure 24: This figure shows the positions of the planet, moon, and submoon with the characteristics given in Table 3 in the x-y plane relative to the star. The simulation was run to 100 years with a timestep of 0.01 years and has the same initial conditions as the trial presented in Figure 23, but the submoon was started at a different point along its orbit. The blue, green, and red points correspond to the planet, moon, and submoon respectively. The submoon is immediately ejected from the system.

Thus, though more testing of the Kepler 1625-bi system is necessary, preliminary results indicate that the planet and moon are stable for up to 10,000 years, while neither a Triton-like nor a Ceres-like submoon is stable over any significant period of time. Overall, these tests of the submoon subroutine show reasonable simulated submoon behavior. The instability of the all three submoons tested is likely a product of the configuration, though errors in the code cannot be ruled out, as there are no known submoons to which to compare their motion. Thus, while more testing of the code is necessary for total confirmation of its validity, preliminary results show reasonable behavior based on the given initial conditions.

4 Discussion and Conclusion

Over the course of this work, the behavior of submoons was modeled using an N-Body code. This was achieved by adding a subroutine which initializes a body orbiting a moon into an existing code that calculates the position, velocity, acceleration, and jerk of N bodies based on their gravitational interactions with each body in the simulation. This approach differs from past submoon investigations, in that it models the bodies in their actual locations with all of the forces they are expected to feel. Other works have focused on finding solutions to highly simplified equations meant to describe the motion of the bodies due to tidal evolution [29, 30, 31]. These solutions do not account for the same factors that an N-body code does, including the influences of the initial planet and moon rotations, the moon on the planet's rotation, or the submoon on the moon's rotation [31]. In addition, these works assumed that the submoons mass was much smaller than that of the moon, which was not done in these simulations [29, 30, 31].

Preliminary results of the N-Body code show that the submoons tested did not occupy stable orbits around their host moons for any significant period of time, but much future work is required to fully confirm these results and the code's validity. Checking the validity of the code's results is especially difficult, as there are no known submoon's whose behavior could be recreated and little work has been done to model fictitious submoons. Thus, in order to more thoroughly understand submoon stability and behavior as well as the code itself, more studies must be conducted, which will need to span a much larger parameter space, including varying the sizes of the bodies involved (planet, moon, submoon), the semi-major axes, and the eccentricities and inclinations of the orbits. Hopefully, as more work is done to study submoons within the general astrophysical community, there will also be more data from other researchers with which to compare this N-Body code's results and through which to better understand submoons.

In addition to a general survey of the various orbital and physical parameters involved in a submoon's behavior and stability, more research should be conducted into how the factors that greatly affect moons would impact submoons. This includes the presence of other bodies in the vicinity of the submoon, such as other submoons, additional moons, or even close-by planets. The impact of migration on submoon stability should also be investigated, as this is believed to be an incredibly common occurrence in late-stage planet formation. In general, the formation of submoons and the planetary formation mechanisms required to form or retain submoons should also be investigated, as future observations regarding the presence of submoons, or lack thereof, could then provide constraints on planet and moon formation processes. Thus, the investigation of submoon behavior in the context of factors that have a large impact on moon formation will become a very important future research field and help to answer remaining questions about planet and moon formation.

Overall, this work provides the tools necessary to begin a more in-depth study of submoons, their behavior and stability, which is highly encouraged in order to better understand the formation and history of both the Solar system and other extrasolar systems.

References

[1] P. Brennan, K. Walbolt, and A. Biferno, "Exoplanet Catalog Reference – Exoplanet Exploration: Planets Beyond our Solar System."

[2] International Astronomical Unions Working Group for Planetary System Nomenclature, "Planetary Names: Planet and Satellite Names and Discoverers."

[3] "5 Ways to Find a Planet Explore – Exoplanet Exploration: Planets Beyond our Solar System."

[4] A. Teachey, "On the Population of Exomoons - in Kepler, and the Exomoon Candidate Kepler-1625B I," *Diversis Mundi: The Solar System in an Exoplanetary Context*, p. 29, jul 2018.

[5] L. Glaze, K. Erickson, P. Davis, and B. Dunford, "By the Numbers Ganymede – NASA Solar System Exploration."

[6] L. Glaze, K. Erickson, P. Davis, and B. Dunford, "By the Numbers Titan ."

[7] L. Glaze, K. Erickson, P. Davis, and B. Dunford, "By the Numbers Callisto ."

[8] L. Glaze, K. Erickson, P. Davis, and B. Dunford, "By the Numbers Neptune ."

[9] R. Heller, "The nature of the giant exomoon candidate Kepler-1625 b-i," tech. rep., 2018.

[10] R. Heller, K. Rodenbeck, and G. Bruno, "An alternative interpretation of the exomoon candidate signal in the combined Kepler and Hubble data of Kepler-1625," *Astronomy and Astrophysics*, vol. 624, p. 8, apr 2019.

[11] A. Teachey and D. M. Kipping, "Evidence for a Large Exomoon Orbiting Kepler-1625b," tech. rep., 2018.

[12] L. Kreidberg, R. Luger, and M. Bedell, "No Evidence for Lunar Transit in New Analysis of Hubble Space Telescope Observations of the Kepler-1625 System," *The Astrophysical Journal Letters*, vol. 877, no. 2, p. 6, 2019.

[13] A. Teachey, D. Kipping, C. J. Burke, R. Angus, and A. W. Howard, "Loose Ends for the Exomoon Candidate Host Kepler-1625b," *The Astronomical Journal*, vol. 159, p. 142, mar 2020.

[14] C. D. Murray and S. F. Dermott, *Solar system dynamics*. Cambridge University Press, 2010.

[15] S. Kohler, "The Impact of Stars on Moons ," jan 2017.

[16] J. W. Barnes and D. P. O'brien, "Stability of Satellites Around Close-in Extrasolar Giant Planets," tech. rep., 2002.

[17] J. A. BURNS, "Where are the Satellites of the Inner Planets?," *Nature Physical Science*, vol. 242, pp. 23–25, mar 1973.

[18] W. R. Ward and M. J. Reid, "SOLAR TIDAL FRICTION AND SATELLITE LOSS," *Monthly Notices of the Royal Astronomical Society*, vol. 164, pp. 21–32, apr 1973.

[19] T. Sasaki, J. W. Barnes, and D. P. O'Brien, "OUTCOMES AND DURATION OF TIDAL EVOLUTION IN A STAR-PLANET-MOON SYSTEM," *The Astrophysical Journal*, vol. 754, p. 51, jul 2012.

[20] Y. Shen and S. Tremaine, "Stability of the Distant Satellites of the Giant Planets in the Solar System," *The Astronomical Journal*, vol. 136, pp. 2453–2467, 2008.

[21] R. C. Domingos, O. C. Winter, and T. Yokoyama, "Stable satellites around extrasolar giant planets," *Monthly Notices of the Royal Astronomical Society*, vol. 373, pp. 1227–1234, dec 2006.

[22] S. N. Raymond and A. Morbidelli, "Planet formation: key mechanisms and global models," tech. rep., 2020.

[23] F. Namouni, "The Fate of Moons of Close-In Giant Exoplanets," *The Astrophysical Journal Letters*, vol. 719, no. 2, pp. 145–147, 2010.

[24] C. Spalding, K. Batygin, and F. C. Adams, "RESONANT REMOVAL OF EXOMOONS DURING PLANETARY MIGRATION," tech. rep., 2018.

[25] Y.-C. Hong, S. N. Raymond, P. D. Nicholson, and J. I. Lunine, "Innocent Bystanders: Orbital Dynamics of Exomoons During Planet–Planet Scattering," *The Astrophysical Journal*, vol. 852, p. 85, jan 2018.

[26] A. C. Barr and M. B. Syal, "Formation of Massive Rocky Exomoons by Giant Impact," tech. rep., 2017.

[27] S. Kohler, "The Fate of Exomoons when Planets Scatter," mar 2018.

[28] A. S. Hamers, M. X. Cai, J. Roa, and N. Leigh, "Stability of exomoons around the Kepler transiting circumbinary planets," tech. rep., 2018.

[29] M. J. Reid, "The Tidal Loss of Satellite-Orbiting Objects and Implications for the Lunar Surface," tech. rep., 1973.

[30] B. A. Conway, "Stability and evolution of primeval lunar satellite orbits," *Icarus*, vol. 66, pp. 324–329, may 1985.

[31] J. A. Kollmeier and S. N. Raymond, "Can Moons Have Moons?," tech. rep., 2019.

[32] J. M. A. Danby, *Fundamentals of celestial mechanics*. Willmann-Bell, 1988.

[33] S. G. Alexander and C. B. Agnor, "N-Body Simulations of Late Stage Planetary Formation with a Simple Fragmentation Model," *Icarus*, vol. 132, pp. 113–124, mar 1998.

[34] C. Fuse and J. Spiegelberg, "Formation of Ice Giant Satellites During Thommes Model Migration," *AAS*, vol. 231, p. 144.16, 2018.

[35] L. Glaze, K. Erickson, P. Davis, and B. Dunford, "In Depth — Explorer 35 – NASA Solar System Exploration."

[36] K. Erickson and M. Wasser, "Moon Missions — Exploration – Moon: NASA Science."

[37] L. Glaze, K. Erickson, P. Davis, and B. Dunford, "By the Numbers Ceres."